









## ARTICLE

# Distinct timescales of RNA regulators enable the construction of a genetic pulse generator

Alexandra Westbrook<sup>1\*</sup>  | Xun Tang<sup>2\*</sup>  | Ryan Marshall<sup>3</sup> | Colin S. Maxwell<sup>4</sup>  |  
James Chappell<sup>5</sup>  | Deepak K. Agrawal<sup>6</sup> | Mary J. Dunlop<sup>6</sup>  | Vincent Noireaux<sup>3</sup>  |  
Chase L. Beisel<sup>4,7,8</sup>  | Julius Lucks<sup>9†</sup>  | Elisa Franco<sup>2†</sup> 

<sup>1</sup>Robert F. Smith School of Chemical and Biomolecular Engineering, Cornell University, Ithaca, New York

<sup>2</sup>Department of Mechanical Engineering, University of California at Riverside, Riverside, California

<sup>3</sup>School of Physics and Astronomy, University of Minnesota, Minneapolis, Minnesota

<sup>4</sup>Department of Chemical and Biomolecular Engineering, North Carolina State University, Raleigh, North Carolina

<sup>5</sup>Department of Biosciences, Rice University, Houston, Texas

<sup>6</sup>Biomedical Engineering Department, Boston University, Boston, Massachusetts

<sup>7</sup>Helmholtz Institute for RNA-based Infection Research (HIRI), Helmholtz-Centre for Infection Research (HZI), Würzburg, Germany

<sup>8</sup>Faculty of Medicine, University of Würzburg, Würzburg, Germany

<sup>9</sup>Department of Chemical and Biological Engineering, Northwestern University, Evanston, Illinois

**Correspondence**

Elisa Franco, Department of Mechanical Engineering, University of California at Riverside, Riverside, CA 92521.

Email: efranco@engr.ucr.edu

**Funding information**

Defense Advanced Research Projects Agency, Grant/Award Numbers: HR0011-16-C-01-34, HR0011-16-C-01-34

**Abstract**

To build complex genetic networks with predictable behaviors, synthetic biologists use libraries of modular parts that can be characterized in isolation and assembled together to create programmable higher-order functions. Characterization experiments and computational models for gene regulatory parts operating in isolation are routinely used to predict the dynamics of interconnected parts and guide the construction of new synthetic devices. Here, we individually characterize two modes of RNA-based transcriptional regulation, using small transcription activating RNAs (STARs) and clustered regularly interspaced short palindromic repeats interference (CRISPRi), and show how their distinct regulatory timescales can be used to engineer a composed feedforward loop that creates a pulse of gene expression. We use a cell-free transcription-translation system (TXTL) to rapidly characterize the system, and we apply Bayesian inference to extract kinetic parameters for an ordinary differential equation-based mechanistic model. We then demonstrate in simulation and verify with TXTL experiments that the simultaneous regulation of a single gene target with STARs and CRISPRi leads to a pulse of gene expression. Our results suggest the modularity of the two regulators in an integrated genetic circuit, and we anticipate that construction and modeling frameworks that can leverage this modularity will become increasingly important as synthetic circuits increase in complexity.

**KEYWORDS**

Bayesian methods, CRISPRi, model-guided design, RNA-based circuits, sRNA

## 1 | INTRODUCTION

An important goal of synthetic biology is the development of rational methods for precise temporal control of gene expression, which is

necessary to achieve sophisticated dynamic functions in engineered cells (Gupta, Reizman, Reisch, & Prather, 2017). Toward this broad goal, libraries of synthetic regulatory parts have been developed to give synthetic biologists control over distinct levels of gene expression (Chappell, Westbrook, Verosloff, & Lucks, 2017; Green, Silver, Collins, & Yin, 2014). To create more complex networks, these parts need to be modular and composable (Lucks, Qi, Whitaker, & Arkin, 2008), performing their function within the network with

\*Alexandra Westbrook and Xun Tang are considered co-first author.

†Elisa Franco and Julius Lucks are considered joint senior author.

minimal undesired interactions. RNA provides a powerful platform to achieve this.

RNA-based regulators have become increasingly popular for building libraries of synthetic parts to orthogonally control many aspects of gene expression (Carrier & Keasling, 1999; Chappell et al., 2013; Chappell et al., 2017; Green et al., 2014; Lucks, Qi, Mutalik, Wang, & Arkin, 2011), RNA transcriptional regulators are particularly interesting because they can regulate RNA synthesis as a function of a RNA input and thus can be used to create genetic circuitry that propagates signals on the RNA level (Lucks et al., 2011; Takahashi, Chappell et al., 2015). These circuits have many potential advantages over protein-based circuits, including the ability to leverage RNA-folding algorithms and high-throughput structure determination to optimize regulatory part folding and function (Takahashi et al., 2016), to reduce metabolic load for the host (Beisel & Storz, 2010), and to allow rapid signal propagation due to their fast degradation rates (Takahashi, Chappell et al., 2015).

Here we focus on building a simple genetic network by combining two modes of RNA-based transcriptional regulation: using small transcription activating RNAs (STARs; Chappell, Takahashi, & Lucks, 2015) and clustered regularly interspaced short palindromic repeats interference (CRISPRi; Bikard et al., 2013; Qi et al., 2013). STARs activate gene expression through an interaction with a sequence specific target RNA. The target RNA resides in the 5'-untranslated region (5'-UTR) of the gene of interest and folds into a transcriptional terminator that halts transcription by causing the polymerase to fall off of the DNA complex before the downstream gene. When present, the activating RNA—called the STAR—binds to the target RNA to prevent terminator formation, thus allowing downstream transcription to turn gene expression ON (Figure 1a). Libraries of orthogonal STARs have been built and shown to work in many contexts, including within genomic DNA to reprogram cellular phenotypes, and to control multiple genes within a metabolic pathway (Chappell et al., 2015; Chappell et al., 2017).

CRISPRi is a method of transcriptional repression that relies on targeting a catalytically dead Cas9 (dCas9) nuclease to a gene (Qi et al., 2013). Targeting is dictated by a guide RNA (gRNA) with a short segment that is complementary to the sequence of interest. Here we use the *Streptococcus pyogenes* Cas9 that targets sequences flanked by a 3' NGG PAM. Binding of the dCas9:gRNA ribonucleoprotein complex to DNA can either block polymerase binding if the targeted region is near a promoter or halt transcription elongation if the targeted region is within a gene. Orthogonal gRNAs can be designed to independently regulate multiple genes or to integrate signals for genetic circuits such as logic gates (Gander, Vrana, Voje, Carothers, & Klavins, 2017). In nature, gRNAs are produced by RNase III cleavage of double stranded RNA formed by the binding of a trans-activating CRISPR RNA (tracrRNA) to complementary sequences in a transcribed CRISPR RNA (Deltcheva et al., 2011). The resulting processed CRISPR RNA (crRNA) binds to Cas9 (or dCas9) to form an active ribonucleoprotein complex (Figure 1b). CRISPRi works efficiently using either gRNAs produced by the processing of crRNA/tracrRNA duplexes or using single-guide RNAs

which fuse the tracrRNA and crRNA to mimic the processed form using a single molecule (Jinek et al., 2012). In this study we use separate crRNA and tracrRNA because they represent the natural form of the gRNA as it is expressed in bacteria, and they also add to an additional time delay in the CRISPRi regulation due to the kinetics of pairing between the RNAs.

One difference between STAR and CRISPRi mechanisms is the timescale on which the regulation occurs. STARs rely on one cotranscriptional RNA-RNA interaction that results in transcription activation typically within minutes (Chappell et al., 2017), while CRISPRi requires the formation of a RNA-protein repressor complex before binding to DNA for repression, which has been shown to take on the order of 1 hr for regulation to occur (Qi et al., 2013). This timescale difference between these two opposing modes of gene regulation thus creates an intriguing possibility to use STARs and CRISPRi to engineer a network that produces a pulse of gene expression, similar to the incoherent type-1 feedforward loop (I1-FFL; Mangan & Alon, 2003).

The I1-FFL is a common network motif in natural bacterial networks (Alon, 2013; Milo et al., 2002; Shen-Orr, Milo, Mangan, & Alon, 2002) and has received much interest due to its ability to produce a pulse of gene expression (Basu, Mehreja, Thiberge, Chen, & Weiss, 2004; Mangan & Alon, 2003) and accelerate the response time (Mangan, Itzkovitz, Zaslaver, & Alon, 2006). I1-FFLs have also been used to implement band-pass filters (Entus, Aufderheide, & Sauro, 2007; Kaplan, Bren, Dekel, & Alon, 2008), fold-change detection (Goentoro, Shoval, Kirschner, & Alon, 2009), biosensing (Barone et al., 2017), and noise buffering (Osella, Bosia, Corá, & Caselle, 2011). An I1-FFL consists of an activator X that activates a gene Z and simultaneously its repressor, Y (Figure 1c). It can produce a pulse of gene Z expression because the activation reaction is triggered immediately by X, while the dominating repression occurs with a delay due to the presence of the intermediate component Y (Mangan & Alon, 2003). Here, we exploit STARs to induce rapid activation of gene expression, and CRISPRi to achieve delayed repression due to the slow assembly of the gRNA-dCas9 complex. We expect that, when combined, these two RNA-based regulatory mechanisms will operate on timescales that are sufficiently different to yield a transient pulse of gene expression (Figure 1d). While our design is not an I1-FFL by a strict definition, it accomplishes the same general behavior and should produce a pulse of gene expression by exploiting the regulatory timescale differences to cause the delayed repression of Z after fast activation.

A challenge in interconnecting molecular components characterized in isolation is that unexpected interactions between species and resource competition can affect the predicted operation of the composed system, as demonstrated previously (Qian, Huang, Jiménez, & Del Vecchio, 2017). Reaction rates can be affected by possible crosstalk between the components and the relative abundance of RNA species and dCas9, which are subject to biological noise and circuit complexity (Mishra, Rivera, Lin, Del Vecchio, & Weiss, 2014), thus making the prediction of the integrated construct dynamics necessary and challenging. To address these challenges, we

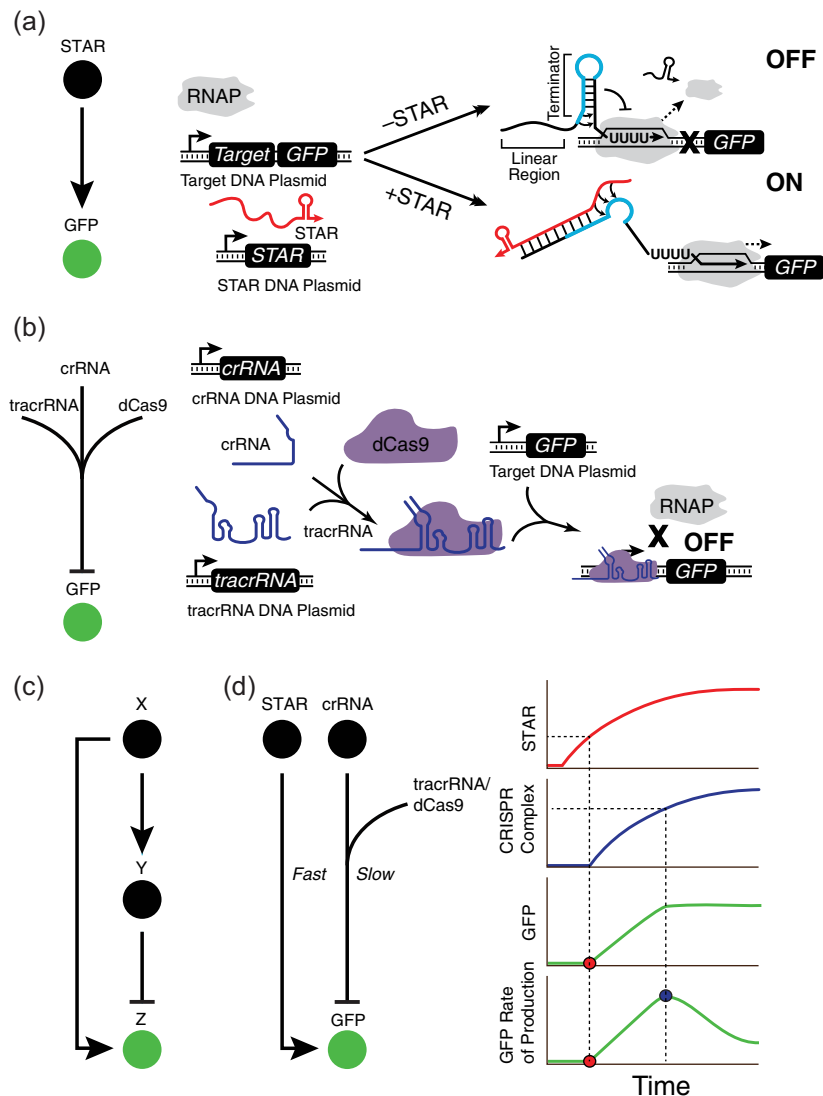


**FIGURE 1** Architecture of a I1-FFL composed of STAR activation and CRISPRi repression. (a) STAR mechanism. The target RNA sequence folds into a transcriptional terminator (blue) that causes RNA polymerase to ratchet off the DNA complex and halt transcription upstream of the gene (gene OFF). When present, a STAR (red) binds to both the linear region and the 5' half of the terminator hairpin (blue) of the target RNA, preventing terminator formation and allowing transcription elongation of the gene (gene ON). (b) CRISPRi mechanism. The crRNA, tracrRNA, and dCas9 bind to form the CRISPR complex that specifically binds to a DNA sequence encoded by the crRNA sequence. When bound the CRISPR complex either blocks transcription initiation or transcription elongation. (c) The I1-FFL motif consists of three parts. An activator X activates expression of Z and its repressor, Y. (d) The pulse generator circuit works by taking advantage of fast STAR activation and slow CRISPRi repression. STAR activates GFP expression immediately while the crRNA/tracrRNA/dCas9 formation causes a delay before finally repressing GFP expression. In TXTL there is no protein degradation, so this causes a pulse in the rate of GFP production. CRISPRi: clustered regularly interspaced short palindromic repeats interference; crRNA: CRISPR RNA; dCas9: dead Cas9; GFP: green fluorescent protein; I1-FFL: type 1 incoherent feedforward loop; STAR: small transcription activating RNA; tracrRNA: trans-activating crRNA; TXTL: transcription-translation system [Color figure can be viewed at [wileyonlinelibrary.com](http://wileyonlinelibrary.com)]

use an interdisciplinary approach that combines cell-free experiments and mathematical modeling.

Mathematical models have gained popularity in guiding the construction and characterization of dynamic molecular systems, given their cost-effectiveness and efficiency as compared with experiments (Hu, Varner, & Lucks, 2015; Liao, Blanchard, & Lu, 2017; Nielsen et al., 2016; Duschak, 2015). Ordinary differential equations (ODEs) are an effective tool to model molecular reaction networks, gene expression in protein-based genetic network systems

(Alon, 2013; Del Vecchio & Murray, 2017), and small RNA transcriptional circuits (Hu et al., 2015; O'Brien, Itallie, & Bennett, 2012). ODEs are particularly suitable to model and parameterize cell-free reactions, where initial concentration of chemical species can be accurately controlled. To rapidly characterize the STAR and CRISPRi reactions we developed ordinary differential equation (ODE) models based on experiments performed with transcription-translation system (TXTL), an *Escherichia coli* cell-free transcription-translation platform (Sun et al., 2013). TXTL experiments have been successfully

combined with mathematical models to parameterize and understand RNA circuits (Agrawal et al., 2018; Hu et al., 2015; Hu, Takahashi, Zhang, & Lucks, 2018). TXTL is ideal for prototyping genetic circuit dynamics because it is quick and easy to use, requires minimal cloning, and shows good agreement with in vivo data (Takahashi, Hayes et al., 2015), and recently it was used to characterize CRISPR nucleases and gRNAs (Marshall et al., 2018). Additionally, TXTL also allows for experiments that would otherwise be difficult to perform in vivo by giving direct control over component concentrations and enabling circuit optimization and flexibility when designing experiments to fit model parameters.

Here, we start by using TXTL to verify that the STAR and CRISPRi present sufficiently distinct regulatory timescales. Then, we build ODE models for the STAR and CRISPRi pathways in isolation, and we perform systematic TXTL experiments to parameterize and validate the models. We find that when the models are composed to build the IFFL circuit, they predict the expected pulse generation. We conclude with experiments showing that, when connected together to regulate the same promoter, the candidate STAR-CRISPRi pulse generator circuit yields a pulse in target gene expression, and that the composed models can quantitatively capture the pulse generator behavior. Our results demonstrate that the combination of modeling and experiments in a simplified TXTL environment is an effective approach to prototyping biological dynamic circuits for control of gene expression. Most importantly, our results indicate that RNA regulators characterized in isolation can be combined in more complex circuits without loss of performance when interconnected, making them modular and composable components for dynamic synthetic circuits.

## 2 | MATERIALS AND METHODS

### 2.1 | Plasmid construction and purification

Key sequences can be found in Supporting Information Table S2. All the plasmids used in this study can be found in Supporting Information Table S3. The STAR plasmid and control plasmid were construct pJBL4971 and pJBL002, respectively, from Chappell et al., (2017). The green fluorescent protein (GFP) expression plasmid was p70a-GFP from Garamella et al. (2016) and the STAR-target plasmid was modified from this plasmid using inverse polymerase chain reaction (iPCR). The plasmids expressing crRNA, tracrRNA, and the scrambled crRNA were constructed using Gibson Assembly and iPCR and sequence verified using sanger sequencing. Plasmids were purified using a Qiagen QIAfilter Plasmid Midi Kit (Catalog number: 12243; Qiagen, Germantown, MD) followed by isopropanol precipitation and eluted with double distilled water.

### 2.2 | TXTL extract and buffer preparation

Cell extract and reaction buffer were prepared according to the previous work (Garamella et al., 2016).

### 2.3 | TXTL experiments

TXTL buffer and extract tubes were thawed on ice for approximately 20 min. Separate reaction tubes were prepared with combinations of DNA representing a given circuit condition. Appropriate volumes of DNA, buffer, and extract were calculated using a custom spreadsheet developed by Sun et al. (2013) and modified to fit the experiments. Buffer and extract were mixed together and then added to each tube of DNA according to the previously published protocol. Each TXTL reaction mixture (10  $\mu$ l each) was transferred into a 384-well plate (Nunc 142761, Thermo Scientific), covered with a plate seal (Nunc 232701, Thermo Scientific), and placed on a Biotek Synergy H1m plate reader (Biotek, Winooski, VT). We note that special care is needed when pipetting to avoid air bubbles, which can interfere with fluorescence measurements. Temperature was controlled at 29°C. GFP fluorescence was measured (485 nm excitation, 520 emission) every 5 min. A calibration to enhanced GFP (EGFP) concentration ( $\mu$ M) was performed using a standard curve of pure EGFP (STA-201; Cell Biolabs, San Diego, CA) to present measurement data in terms of GFP concentration. Preincubation experiments were performed by combining two types of extracts. One extract has dCas9 pre-expressed and the other does not. Each plasmid was incubated in the appropriate extract and buffer for 2 hr before the preincubated reactions were combined in equal parts and measurements began.

### 2.4 | Modeling

Equations in Figure 3 were solved with MATLAB\_R2014b *ode23s* solver to get the simulated GFP concentration for the error calculation (Equation (2)) in data fitting. Candidate parameters were generated with a uniform distribution within a bounded interval (Supporting Information Table S1), using MATLAB random number generation function *rand*. One trial of the Bayesian inference data fitting (i.e., one initial guess, with 105,000 iterations) took about three computational hours on a Macbook Pro with a 2 GHz Intel Core i7 processor. Model in Figure 5 was also numerically solved with MATLAB\_R2014b *ode23s* function to get predictions for the combined pulse generator. MATLAB scripts for the STAR, CRISPRi, and Pulse generator models, as well as the corresponding parameterization are available on GitHub, downloadable at: [https://github.com/XunPSU/Westbrook\\_Tang-et-al-SI-Model-Code.git](https://github.com/XunPSU/Westbrook_Tang-et-al-SI-Model-Code.git)

## 3 | RESULTS

### 3.1 | Preincubation experiments confirm the expected STAR/CRISPRi timescale difference

We first sought to verify the timescale difference between STAR and CRISPRi regulation expected from previous studies (Chappell et al., 2015, 2017). To do this, we designed experiments that isolated the kinetic processes of each mechanism. We transcribed RNA components and allowed folding and complex formation with previously synthesized dCas9 before assessing regulatory function, to isolate only the timescale

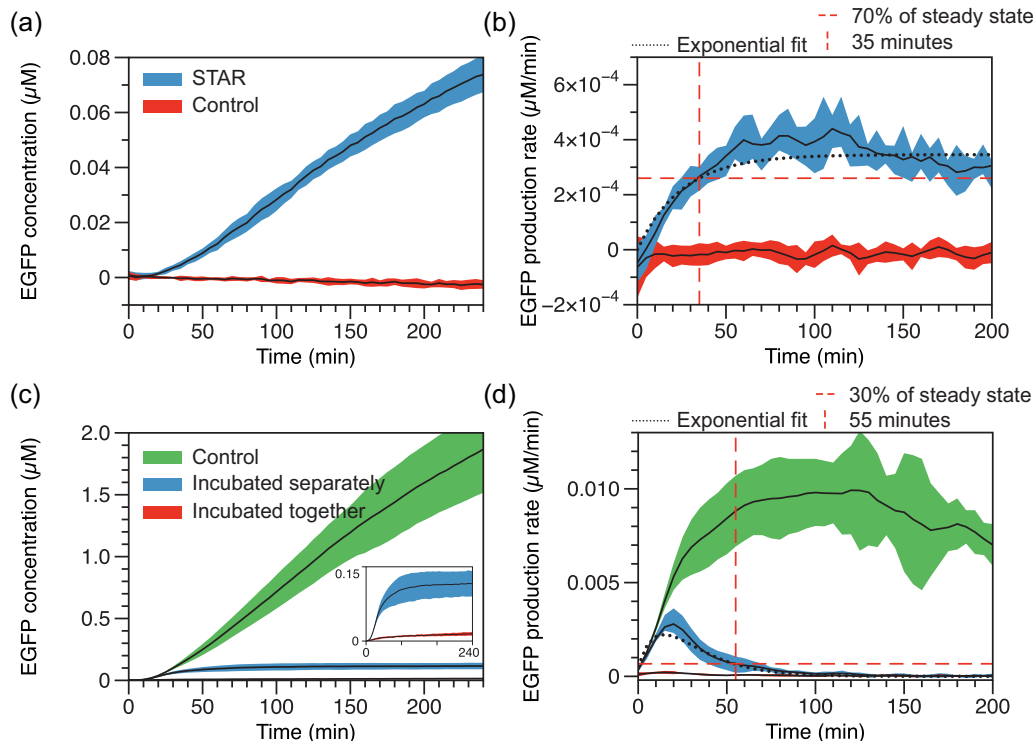


**FIGURE 2** Preincubation experiments indicate that STAR activation is faster than dCas9-based repression. (a) Functional time course characterization of GFP expression when STAR is preincubated (blue) or a nonfunctional control is preincubated (red). The timescale of STAR activation is on the order of 20 min after reporter DNA is added to the reaction. (b) The production rate of GFP expression for the STAR preincubation experiment. The GFP production rate reached 70% of max as determined by the exponential fit (dotted black line) at 35 min. (c) Functional time course characterization of the CRISPRi response when parts are incubated together (red) or separately (blue) in comparison to unrepressed expression (green). The timescale of preincubated CRISPR repression is much faster than when the parts are incubated separately, suggesting that the dCas9 loading time adds a significant delay to the system. The inset shows the two repressed states. Data for all preincubation combinations of CRISPRi parts is shown in Supporting Information Figure S7. (d) The production rate of GFP expression for the CRISPRi preincubation experiment. The GFP production rate reached 30% of its peak as determined by the exponential fit to the derivative (dotted black line) at 55 min. CRISPRi: clustered regularly interspaced short palindromic repeats interference; crRNA: CRISPR RNA; dCas9: dead Cas9; EGFP: enhanced green fluorescent protein green fluorescent protein; STAR: small transcription activating RNA [Color figure can be viewed at [wileyonlinelibrary.com](http://wileyonlinelibrary.com)]

of the regulatory mechanism. When performing a typical TXTL experiment, all DNA is added to the reaction at  $t=0$  and gene expression is measured over the course of a few hours. Inherent to this experimental design is a delay due to the transcription of RNA regulator parts, which must first be transcribed before they can perform their function. To isolate the timescale of the regulatory event, we incubated a plasmid expressing each RNA regulatory part alone for 2 hr, essentially allowing the TXTL reaction to synthesize RNA regulators before being assessed for function. We then mixed preincubated reactions with reporter DNA and characterized the response time of the system. In this way, we removed the timescale needed for regulatory RNA synthesis and instead focused the characterization experiment on the relevant timescales of action for each regulator.

The STAR system only has one trans-acting RNA, so we incubated a plasmid expressing the STAR RNA or a plasmid expressing a nonfunctional control RNA in TXTL for 2 hr. We then added DNA encoding the p70a-Target-GFP plasmid to this reaction mixture at  $t=0$  and began measuring fluorescence over time. We observed detectable STAR activation of gene expression  $\sim 20$  min after the

addition of the GFP plasmid (Figure 2a) and STAR activation as determined by the GFP production rate reached 70% of the steady state after 35 min, where the steady state was computed from an exponential fit (Figure 2b) as described in Supporting Information Note S1.

We anticipated that regulation of gene expression by the dCas9 complex would take significantly longer than the STAR activation, given previous observations suggesting that gRNA loading onto dCas9 takes on the order of  $\sim 1$  hr in the presence of nonspecific RNAs (Mekler, Minakhin, Semenova, Kuznedelov, & Severinov, 2016). As the CRISPRi system requires a crRNA, tracrRNA, and dCas9, a more sophisticated experiment was required to characterize the regulatory timescale. Specifically, we sought to determine the timescale for crRNA-tracrRNA-dCas9 complex assembly required for the dCas9 complex to repress gene expression. To quantitatively estimate this timescale, we incubated the DNA encoding each RNA component in all combinations of alone, together, and in TXTL already containing dCas9 for 2 hr (Supporting Information Figure S1) and then combined them into a final reaction with DNA encoding the

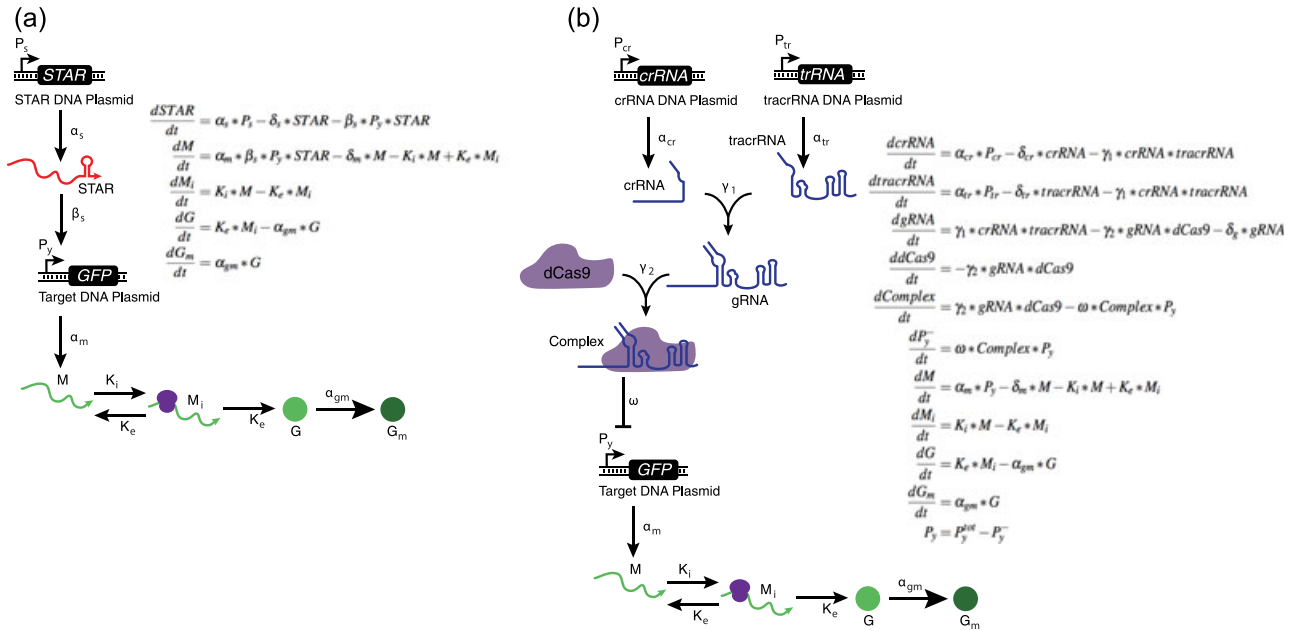


**FIGURE 3** Separate STAR and CRISPRi models with the corresponding topology. The STAR activation is modeled as a one-step binding at rate  $\beta_s$ , to the free output promoter  $P_y$ , to enable expression of GFP messenger RNA  $M$ . The CRISPRi repression is modeled as a two-step reaction, where formation of active repressor complex happens before it binds to the free output promoter  $P_y$  to form the repressed  $P_y^-$ , and GFP is only expressed from the free  $P_y$  promoter. For simplicity, the degradation rates of the RNA species are modeled but not shown in the topology. In both models, mature GFP protein  $G_m$  is compared to experimental measurements. All the STAR,  $M$ ,  $M_i$ ,  $G$ ,  $G_m$ , crRNA, tracrRNA, gRNA, Complex, and  $P_y^-$  are initiated with concentration 0 nM. The initial free  $P_y$  plasmid was 0.5 nM, and dCas9 concentration was estimated to be 35 nM based on previous experimental measurement. CRISPRi: clustered regularly interspaced short palindromic repeats interference; crRNA: CRISPR RNA; dCas9: dead Cas9; GFP: green fluorescent protein green fluorescent protein; gRNA: guide RNA; STAR: small transcription activating RNA; tracrRNA: trans-activating crRNA [Color figure can be viewed at [wileyonlinelibrary.com](http://wileyonlinelibrary.com)]

p70a-GFP plasmid before began measurement. For clarity, we only show two conditions in Figure 2c: all alone or all together in TXTL containing dCas9. When incubated separately, we expect all components to be present at high concentrations at the beginning of the measurement but no CRISPRi repression complex would have formed yet. The complex will begin forming when the measurement starts. When incubated together, we expect the CRISPRi complex to have already formed and be present at high concentrations. Comparing these two conditions indicates the time it takes for the crRNA-tracrRNA-dCas9 complex to form and then repress (Figure 2c). However, when incubated separately, the complex was slower to repress gene expression, and did not achieve full gene repression until 55 min after addition of the DNA reporter construct (Figure 2d). This large difference in response times reveals that the crRNA-tracrRNA-dCas9 complex takes on the order of 55 min to fully form and perform its function in TXTL, which is similar to previous research (Mekler et al., 2016).

Taken together, these results indicate that there is a timescale difference between STAR activation (70% of the steady state production rate seen after 35 min) and CRISPRi repression (30% peak production rate seen after 55 min) due to the extra steps required for the crRNA-tracrRNA-dCas9 complex assembly as opposed to the direct RNA-RNA interactions of the STAR mechanism. These timescale differences could therefore be exploited to construct a simple network architecture that produces a pulse of gene expression.

### 3.2 | STAR and CRISPRi model derivation

After verifying the timescale difference with our preincubation experiments, we then sought to construct mathematical models for the STAR and the CRISPRi systems respectively, to computationally test our hypothesis and guide the design of the circuit before conducting further experiments. We used ordinary differential equations to model the rate-of-change of each molecular concentration, as a result of coupled kinetic reactions (Figure 3).

In the STAR system, messenger RNA (mRNA) is produced when STAR binds to the 5'-UTR, changing its structure allowing RNA polymerase to continue transcription. Given the fact that (a) these reactions only involve RNA-RNA interactions, and (b) the purpose of modeling in this study is to provide a qualitative representation of the process, for simplicity, we modeled the STAR activation as a one-step reaction, where STAR binds to the free promoter  $P_y$  directly to achieve transcription activation, at rate  $\beta_s$ . This is an approximation that coarse-grains the details of how the small RNA modifies target RNA structure to activate transcription, and it is justified based on similar simplifying assumptions made in previous work modeling RNA transcriptional repressors (Hu et al., 2015, 2018). In parallel, we modeled CRISPR-Cas9 complex formation as a two-step reaction process. As the first step of this process, the tracrRNA and the crRNA bind to form the gRNA at rate  $\gamma_1$ , then the gRNA binds to dCas9 to form the active repressor complex at rate  $\gamma_2$ . Since there is no explicit investigation on the CRISPR formation process, the two-step reaction mechanism assumption here

was made based on the crystal structure of the tracrRNA, crRNA, and dCas9 molecules that tracrRNA and crRNA should hybridize first before dCas9 binding. Since dCas9 dissociation rates are extremely low with no mismatches (Boyle et al., 2017; Wright et al., 2015), we assumed the formation of the CRISPR-Cas9 complex and its binding (at rate  $\omega$ ) to the free promoter  $P_\gamma$  to form the repressed promoter  $P_\gamma^-$  to be irreversible. While capturing the key reactions in the CRISPR-Cas9 formation, the model coarse-grains the detailed dynamics of how crRNA, tracrRNA, and dCas9 interact with each other and interferes transcription. To enable a direct comparison between the STAR and CRISPRi regulation pathway, we used a first-order kinetic reaction to model the STAR activation, instead of the Hill-type function used in Hu et al. (2015).

In the STAR system, reporter p70a-Target-GFP mRNA (M) is only produced when p70a-Target-GFP ( $P_\gamma$ ) is activated (i.e., bound to STAR at rate  $\beta_s$ ), at rate  $\alpha_m$ , while in the CRISPRi system, M is only produced from the free promoter p70a-GFP (for simplicity and for later use in the combined model, this is also denoted by  $P_\gamma$ ), at rate  $\alpha_m$ . The GFP translational initiation, elongation, and maturation were modeled following previous work (Hu et al., 2015) and the mature GFP ( $G_m$ ) is compared to the experimental measurement.

In addition to the transcriptional rates above, each RNA species has a degradation rate and each protein species has a translation rate. Specifically,  $\alpha_s$ ,  $\alpha_{cr}$ ,  $\alpha_{tr}$ ,  $\delta_s$ ,  $\delta_{cr}$ ,  $\delta_{tr}$ , and  $\delta_g$  are the transcriptional and degradation rates of STAR, crRNA, tracrRNA, and gRNA,

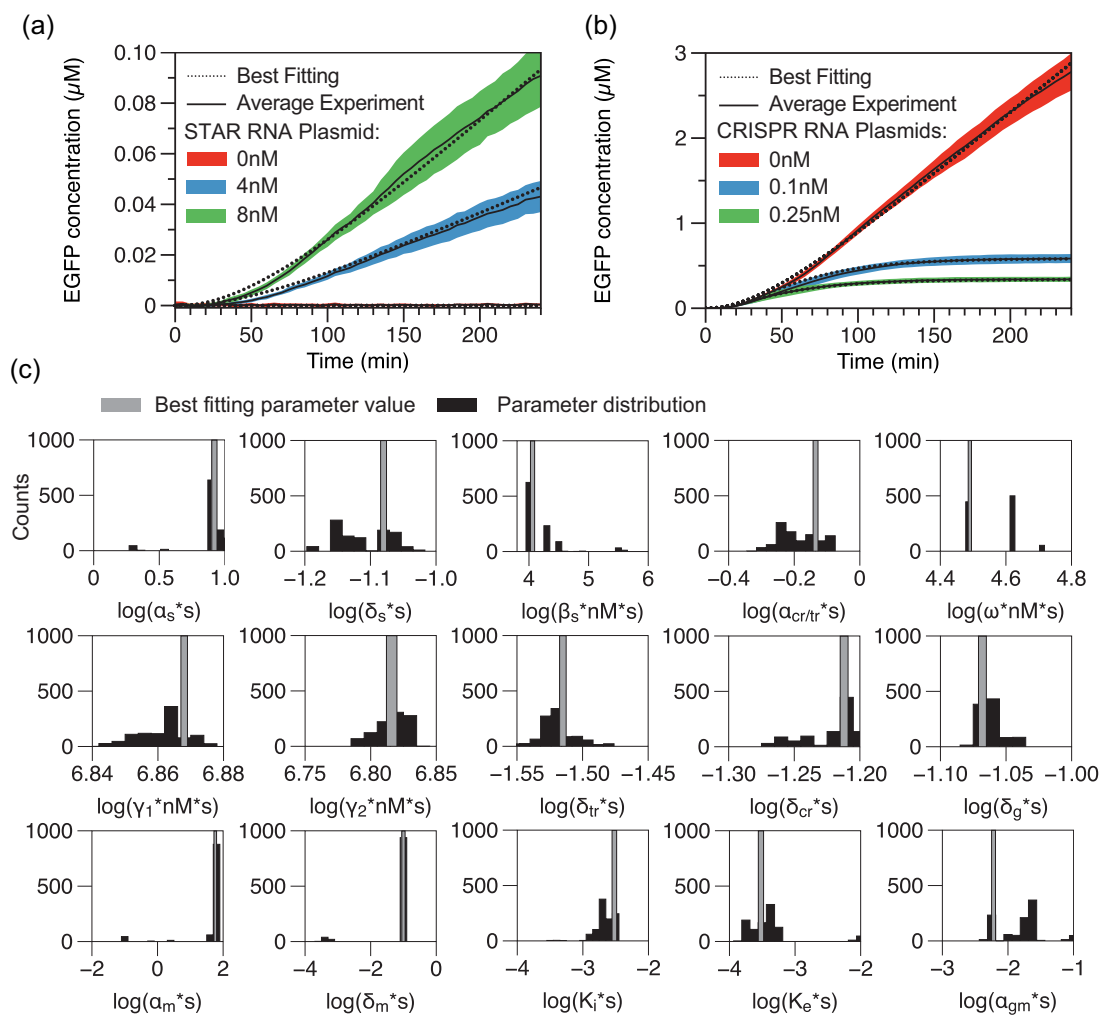


**FIGURE 4** Model parameterization with separate STAR and CRISPRi experiments. (a) Comparison of best-fitted simulation to the STAR experiments for three conditions: high activation with 8 nM of STAR plasmid (green plots, 8 nM STAR), moderate activation with 4 nM of STAR plasmid (blue plots, 4 nM STAR), and no activation with no STAR plasmid (red plots, STAR OFF). (b) Comparison of the best-fitted simulation to the CRISPRi parameterization experiments for three conditions: no repression with no crRNA or tracrRNA (red plots, 0 nM CRISPR RNA), moderate repression with 0.1 nM crRNA and tracrRNA plasmid (blue plots, 0.1 nM CRISPRi RNA), and complete repression with 0.25 nM crRNA and tracrRNA plasmid (green plots, 0.25 nM CRISPRi RNA). (c) Histogram of parameters obtained from 1,000 samples that gave the lowest fitting error within the pool of  $10 \times 105000$  and  $10 \times 210000$  fitting rounds for the STAR and CRISPRi system, respectively. Gray bar indicates the location of the parameter value that gave the best fitting. Note, all the kinetic parameters are scaled to be dimensionless before taking their log values in the histogram plots. CRISPRi: clustered regularly interspaced short palindromic repeats interference; crRNA: CRISPR RNA; EGFP: enhanced green fluorescent protein green fluorescent protein; STAR: small transcription activating RNA; tracrRNA: trans-activating crRNA [Color figure can be viewed at [wileyonlinelibrary.com](http://wileyonlinelibrary.com)]

respectively;  $\delta_m$  is the degradation rate of GFP mRNA,  $M$ ;  $K_i$  is the translation initiation rate,  $K_e$  is the translation elongation rate, and  $\alpha_{gm}$  is the GFP maturation rate.  $P_y^{tot}$  is the total amount of reporter promoters,  $M_i$  is the translationally initialized mRNA, and  $G$  is the immature GFP protein. We note that no protein degradation rate is included because proteins do not degrade in TXTL unless degradation tags are included, (Garamella et al., 2016) and there is no translation rate for dCas9 because extracts were made from *E. coli* cells expressing dCas9 (Marshall et al., 2018).

### 3.3 | Model parameterization

With the separate STAR and CRISPRi models, our next step was to extract suitable kinetic parameters to construct a combined model for reliable predictions. To achieve this, we adopted a Bayesian inference parameterization approach (Brown & Sethna, 2003; Subsoontorn, Kim, & Winfree, 2012) to fit parameters for STARs and CRISPRi separately. A brief summary of this Monte Carlo Bayesian inference approach is given in Supporting Information Note S2; please refer to Subsoontorn et al. (2012), for a complete derivation and discussion of this method. In this study, we used three sets of the STAR activation experiments (full experimental data

shown in Supporting Information Figure S2) to train our model for the three STAR-related kinetic parameters:  $\alpha_s$ ,  $\delta_s$ , and  $\beta_s$ . We also used three sets of the CRISPRi repression experiments (full experimental data is shown in Supporting Information Figure S3) to train our model for the eight CRISPRi-related kinetic parameters:  $\alpha_{cr}$ ,  $\alpha_{tr}$ ,  $\delta_{cr}$ ,  $\delta_{tr}$ ,  $\delta_g$ ,  $\gamma_1$ ,  $\gamma_2$ , and  $\omega$ . As crRNA and tracrRNA were transcribed from the same promoter in our experiments, we assumed that they share the same transcription rate, and we set  $\alpha_{cr} = \alpha_{tr}$  in the fitting. The five reporter GFP-related parameters ( $\alpha_m$ ,  $\delta_m$ ,  $K_i$ ,  $K_e$ , and  $\alpha_{gm}$ ) were also fitted for both STAR and CRISPRi.

For both STAR and CRISPRi experiments, we initiated our fitting with 10 different initial guesses that were evenly spaced in the admissible parameter intervals that were inferred from previous publications (Supporting Information Table S1; Hu et al., 2015). To fit the eight parameters in the STAR model, we conducted 105,000 iterations of parameter updates to seek convergence, and to fit the 12 parameters in the CRISPRi model, we conducted 210,000 iterations. The probability of accepting parameter set  $i$  from parameter set  $j$  was set according to the following (Subsoontorn et al., 2012):

$$P(i \leftarrow j) \begin{cases} e^{-\frac{E_i - E_j}{T}}, & \text{if } \Delta E = E_i - E_j \geq 0, \\ 1, & \text{otherwise} \end{cases} \quad (1)$$

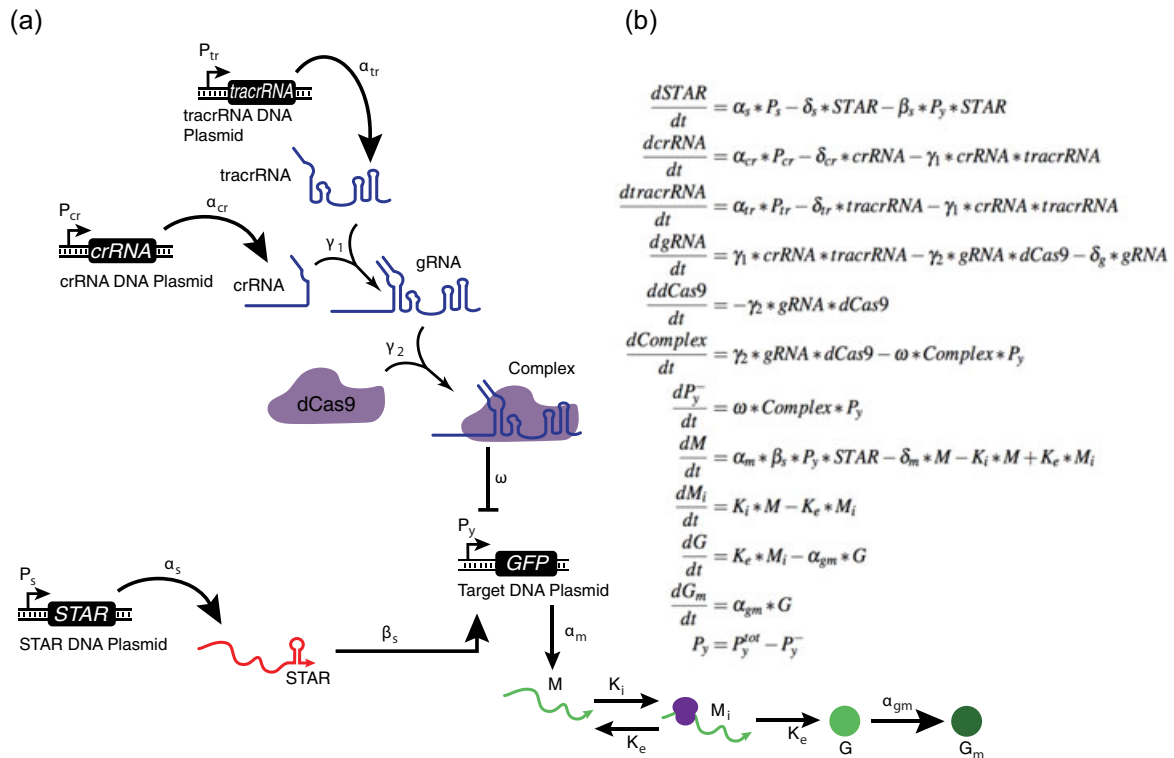


**FIGURE 5** Topology of the pulse generator model. The separate STAR and CRISPRi model are combined by introducing a competition for  $P_y$  binding through the repressor formation in  $dP_y^-/dt$  and the activation in  $dM/dt$  equations. Once CRISPRi repressor complex binds to  $P_y$  to form repressed state  $P_y^-$ , it can no longer be activated for expression.  $P_y$  and  $P_y^-$  follows mass balance with a total initial concentration of  $P_y^{tot}$ . For simplicity, the degradation rates of the RNA species are modeled but not shown in the topology. All the STAR,  $M$ ,  $M_i$ ,  $G$ ,  $G_m$ , crRNA, tracrRNA, gRNA, Complex, and  $P_y^-$  are initiated with concentration 0 nM. The initial free  $P_y$  plasmid was 0.5 nM, and the dCas9 concentration was estimated to be 35 nM based on previous experimental measurement. CRISPRi: clustered regularly interspaced short palindromic repeats interference; crRNA: CRISPR RNA; gRNA: guide RNA; STAR: small transcription activating RNA; tracrRNA: trans-activating crRNA [Color figure can be viewed at wileyonlinelibrary.com]



with  $T = 0.125 (=2\sigma^2)$ , and  $\sigma$  is the estimated measurement error. The cost function  $E$  is defined as the cumulated point-wise squared prediction-measurement error for each experiment cycle:

$$E = \sum_{t=t_0}^{t_f} [\text{Prediction}(t) - \text{Measurement}(t)]^2. \quad (2)$$

The parameter set that gave the lowest cost function  $E$  across all the fittings was deemed as the best-fitted parameter set. The corresponding simulations are plotted in Figure 4a,b against the experimental measurement. The comparisons between predictions and data demonstrate that models trained with the Bayesian inference approach were able to reproduce the dynamics of the STAR and the CRISPRi system under various conditions. To understand the distribution of each parameter, we ranked all the sampled parameter sets (i.e.,  $10 \times 105,000$  and  $210,000$  sets of parameters for the STAR and CRISPRi fitting, respectively) with respect to the corresponding value of the cost function  $E$ . Figure 4c shows the parameter distribution of the first 1,000 sets of parameters that gave the lowest fitting error  $E$ . Note that the five GFP-related parameters shown in Figure 4c were fitted from the STAR activation experiments, for demonstration. The values of the best fitting parameters are given in Supporting Information Table S1.

Interestingly, while some CRISPRi-related parameters have a relatively wide distribution, we see limited variation in the repressor formation-related parameters such as  $\omega$  for the plotted 1,000 fitted parameter values. This observation suggests that the repressor formation kinetics dominate the accuracy of the CRISPRi regulation process. On the other hand, all three STAR-related parameters displayed a relatively wide distribution, which suggests the existence of multiple optimal solutions for the fitting. This might be due to our simplification of the STAR activation mechanism and/or limited experimental conditions (e.g., initial concentrations), such that a wide range of parameter values can fit well the model. Note that fewer reaction steps and experimental conditions lead to fewer constraints for the parameterization. The corresponding parameter distribution of the 1,000 sets that gave the lowest fitting error, and the parameter pair-wise correlation are given in Supporting Information Figures S4 and S5. Detailed sensitivity analysis is included in Supporting Information Figure S6 with respect to: (a) sensitivity analysis in terms of fitting error, subjects to a variation of  $\pm 5\%$  in the nominal values for all three models; (b, c) eigenvalue and projection in the first two components from principal component analysis, with the same 1,000 sets of parameters. All the results did not indicate strong correlations among the parameters.

### 3.4 | Pulse generator modeling and experimental verification

After parameterizing the separate STAR and CRISPRi models, we then combined them to build the pulse generator model by introducing a competition for  $P_y$  promoter binding between STAR and CRISPRi (Figure 5). In the combined pulse generator model, a

free promoter  $P_y$  can either bind to CRISPRi to form a repressed state or to STAR to form an activated state for gene expression. Once  $P_y$  is bound to the CRISPRi complex, it becomes unavailable for STAR activation. To simulate the model, all output promoter copies were initiated in the free state (unbound), with a fixed concentration to mimic conditions used in the CRISPRi characterization experiments.

We then used the combined model to test if a pulse could be generated in the production rate of the target gene. Instead of using one best-fitted parameter set, we decided to combine the set of best fit from each of the 10 Bayesian fittings for both the STAR and the CRISPRi regulator experiments, obtaining 100 sets of parameters (10 STAR  $\times$  10 CRISPRi) to generate predictions of the pulse generator behavior. This is because a mismatch between our model prediction and the pulse generator behavior could be caused by the fact that multiple optimal parameters exist for each individual regulator model (Figure 4), so the combination of the very best fits might not give the most accurate prediction for the interconnected circuit. The procedure to generate combinations of best fits is summarized in Figure 6a. Prediction with the best STAR and CRISPRi separately fitted parameters demonstrated a plateau in the GFP concentration (dashed black plot in Figure 6b), and a pulse in the production rate (dashed black plot in Figure 6c), and indeed all 100 parameter combinations suggested a pulse in the production rate (Supporting Information Figure S7). Given these observations, we expect the integrated pulse generator to function robustly and also to produce a pulse in experiments.

We then performed a TXTL experiment that combined both the STAR and the CRISPRi systems. As in the separate CRISPRi experiment, we added 0.25 nM crRNA, 0.25 nM tracrRNA, and 0.5 nM p70a-Target-GFP. Since the STAR ON expression level is significantly lower than that of the CRISPRi system (Figure 4), we doubled the amount of STAR plasmid used in the separate STAR experiment from 8 nM to 16 nM in the combined system, to mitigate this difference. After the addition of all DNAs, we immediately began measuring fluorescent GFP expression (Figure 6d). As predicted, the experiments also demonstrated a plateau in GFP expression level (Figure 6d, purple), and a pulse in the production rate (Figure 6e, purple). We only see a pulse in the production rate because TXTL has negligible protein degradation (Sun et al., 2013). Only the full pulse generator shows a pulse. Conditions missing either STAR or crRNA show no activation (Figure 6d,e, green and red) or constant activation (Figure 6d,e, blue) indicating that CRISPR regulation, STAR regulation, and their timescale mismatch are necessary for the pulse to occur. If performed in vivo, we would expect a pulse in concentration rather than production rate. We then quantified the prediction accuracy by defining the prediction error in the same way as the cost function in (1) to study the possible changes in the model parameters caused by the combination. The log-based prediction errors are summarized in the heat map in Figure 6f.

One interesting observation is that the best prediction (solid black plot in Figure 6b,c) was not achieved by the set of the best-fitted parameters (dashed black plot). The best-fitted parameter set predicted a higher steady-state concentration in GFP and a taller

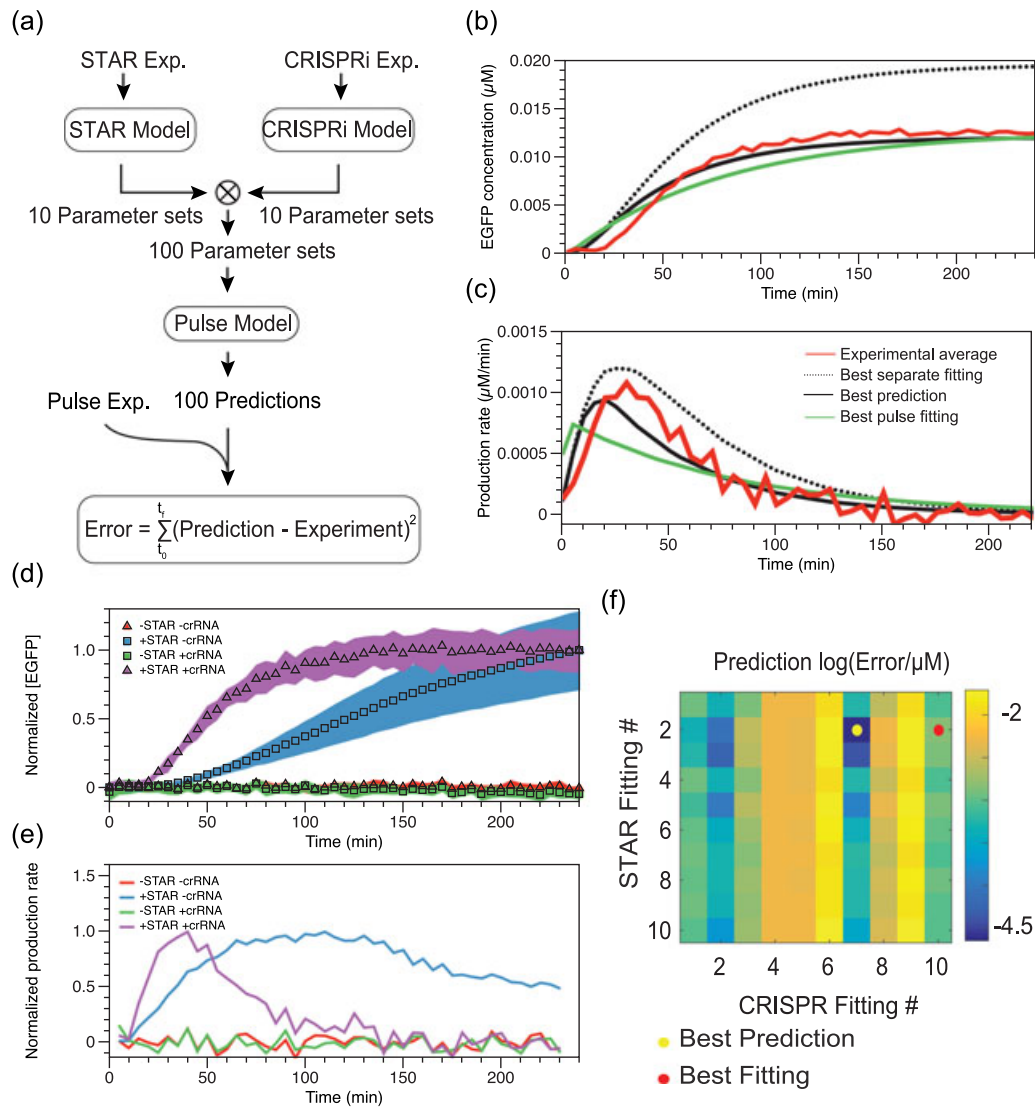


**FIGURE 6** Pulse model prediction and experimental verification. (a) Procedure for parameterization and prediction: each of the individual STAR and CRISPRi models were trained with experimental measurements to fit 10 sets of best fitting parameters. These parameters were then combined into 100 sets that were used to predict the dynamics of the pulse model. The predictions were then compared to experimental measurement and quantified by the squared error between the prediction and the observed trajectories. (b) GFP concentration reached steady state in both the simulation (black and green) and experiments (red) within 240 min, while the best-fitted parameter set predicted a higher steady state concentration level (dashed black), and the best prediction from the separately fitted parameters (solid black) gave better accuracy to the best fitting of the pulse model (green). (c) GFP production rate demonstrated a pulse which peaked at around 40 min and dropped when the repression kicked in and RNA degradation took over, in both the simulations (black and green) and the experiments (red). (d) Functional time course characterization of pulse generator with 0.5 nM of the p70a-STAR Target-GFP plasmid, 16 nM of STAR plasmid (for the +STAR conditions), and 0.25 nM of crRNA and tracrRNA plasmids (for the +crRNA conditions). The pulse generator activates expression and plateaus quickly. GFP does not degrade in TXTL so the pulse is seen in the production rate rather than GFP concentration. The pulse generator (+STAR +crRNA, purple), negative control (-STAR -crRNA, red), and CRISPRi control (-STAR +crRNA, green) conditions are normalized by the +STAR +crRNA and the STAR control (+STAR -crRNA, blue) is normalized by its own maximum. The colored regions (top) indicate the standard deviation of nine replicates. (e) Functional time course characterization of pulse generator production rates. A pulse is generated in production rate when both STAR and crRNA are present (+STAR +crRNA, purple). The production rates shown are smoothed averages of nine replicates. Normalization and standard deviations are done as in part (e). (f) Presentation of the prediction accuracy with the 100 sets of separately fitted parameters indicates the best separately fitted parameter set did not give the best prediction in the combined pulse model. Red dot indicates the location of the best separately fitted parameter set and the yellow dot indicates the location of the parameter set for the best prediction. Note that they are in the same row (i.e., same STAR fitting trial) but different columns (i.e., different CRISPR fitting trial). Best separate fitting: prediction with parameters that best fit the STAR and CRISPR system individually; best prediction: the best of the 100 predictions with individually fitted parameters; best pulse fitting: best out of the 10 fittings to the pulse experiments. CRISPRi: clustered regularly interspaced short palindromic repeats interference; crRNA: CRISPR RNA; gRNA: guide RNA; STAR: small transcription activating RNA [Color figure can be viewed at [wileyonlinelibrary.com](http://wileyonlinelibrary.com)]

pulse in the production rate, as compared with the averaged experimental measurement (solid red plot in Figure 6b,c) and the best prediction. Indeed, the best fitted and the best prediction parameters were from the same STAR (same row in Figure 6f) but a different CRISPRi fitting trial (different column in Figure 6f). The values of the best prediction parameters are given in Supporting Information Table S1. This observation suggested that the coupling may affect the CRISPRi dynamics, such that the set of parameters fit best the separate experiments but underpredicted the repressor formation rate, which lead to a higher predicted GFP expression level. A detailed parameter-to-parameter comparison between the best prediction and the best-fitted parameters is given in Supporting Information Figure S8, to visualize the relative location of each parameter value.

We next asked how well we can fit the STAR/CRISPRi combined model to the experimental measurements, and how that compares to the best prediction with the separately fitted parameters. Again, to seek convergence we conducted 10 Bayesian fittings from different initial guesses, with 210,000 iterations for each fitting (same as in the CRISPRi fitting). The fitting that yielded the lowest fitting error is plotted in Figure 6b,c in green. Surprisingly, the best prediction with the separately fitted parameters slightly outperformed the best fits on the combined model. This could be due to the fact that in the combined model more parameters have to be simultaneously fitted relative to the individual component models, leading the combined model to require a larger number of samplings (i.e., initial guesses and/or iterations) to reach an equally good fit. Indeed, the fitting error comparison in Supporting Information Figure S9 suggests that to fit 12 parameters in the CRISPRi model, even more iterations might be needed. Additionally, the best prediction from the separately fitted parameters is similar to the best fits out of 100 fittings, since it is the best prediction from a  $10 \times 10$  best-fitted parameter sets. To improve the fitting on the combined model, one can use more initial guesses and increase the number of iterations. Supporting Information Figure S9 summarizes the detailed comparison of the accuracy and the error convergence for the STAR, CRISPRi, and pulse generator model fitting, respectively.

## 4 | DISCUSSION

In this study we have demonstrated a RNA-based pulse generator in TXTL that harnesses the difference in speed between STAR and CRISPRi regulation. This STAR-CRISPRi hybrid construct is able to produce a pulse of gene expression. STAR activation involves a single, fast, cotranscriptional RNA-RNA interaction while CRISPRi requires the slow formation of an RNA-protein complex leading to a delay before CRISPRi repression sets in. Combined, these mechanisms produce pulse of gene expression caused by the transcription of a few RNA molecules.

There have been a number of synthetic I1-FFLs built using protein regulators (Barone et al., 2017; Cheng, Hirning, Josić, & Bennett, 2017; Entus et al., 2007). Recently, we built a RNA-based I1-

FFL that uses *N*-acyl homoserine lactone to activate expression of a STAR RNA that activates expression of monomeric red fluorescent protein (mRFP) as well as a gRNA and dCas9 that repress mRFP (Chappell et al., 2017). This design relies on an additional RNA cleavage strategy, cascading RNA regulatory events, and slow dCas9 production. Here, we constructed a simpler network that implements the pulse of gene expression of an I1-FFL but faster and more effectively with a simpler network design.

As synthetic networks grow in complexity, models will be vital for predicting their behavior and understanding dynamics, as they provide faster assessments of the network as compared with experiments. Here, we constructed and parameterized a coarse-grained mechanistic model and used it to predict the dynamics of the pulse generator network. With the simulation results, we observed possible modularity of the STAR regulator when combined with other structures to form more complicated networks, while the performance of the CRISPRi regulation might be affected, as indicated by the change in the parameter values. However, this observed change in the CRISPRi regulation might be due to several reasons: first, given the limited amount of training data, it could be possible that the CRISPRi parameters were over-fitted on the training data thus giving a nonideal prediction in the new condition (combined system). Indeed, the complexity, parameterization methods, and experimental noise could all contribute to the accuracy of the model parameterization. Second, unmodeled (and undesired) coupling of the two regulatory pathways could affect the dynamics; for example, indirect competition for the transcription machinery could reduce transcription rates in a nonhomogeneous manner in the two circuits, altering their regulation timescale. Third, the mechanism of the CRISPRi repressor formation might be oversimplified such that intermediate reaction steps were overlooked. For further investigations, we suggest a richer data set under various conditions for model parameterization, and a refined model to encompass more detailed reactions in the system.

Model parameterization can be challenging, especially when obtaining large amount of experimental measurements under various conditions is costly and a stochastic parameterization method is used, which would normally require convergence. The results in this study suggest that, instead of fitting all the parameters simultaneously, fitting part of a combined network separately could also lead to reliable predictions of an integrated structure, especially when the modularity of each component can be maintained. Because fitting parameters of individual modules for use in integrated structures provides a more computationally tractable alternative to comprehensive parameter fitting, we expect this approach to become predominant as synthetic molecular systems become more and more complex.

In summary, we demonstrate a STAR-CRISPRi hybrid pulse generator both with simulation and in vitro TXTL experiments; the circuit mimics the architecture and performance of an I1-FFL. We also demonstrated how mathematical modeling can be used to guide and assess the design of biological constructs. We found that parameters fitted from separate models can also accurately predict

the performance of the combined model/construct. We further discussed the importance of sample data, and optimization settings in improving the parameterization. We anticipate the results in this study to provide guideline for future work in the modeling, parameterization, and construction of biological parts made of both STAR and CRISPRi regulators.

## ACKNOWLEDGMENTS

This study was supported by the Defense Advanced Research Projects Agency (contract HR0011-16-C-01-34). A. W., X. T., R. M., C. M., J. C., D. A., M. D., V. N., C. B., J. L., and E. F. all contributed to the conception and design and participated in revision of the manuscript. E. F. and J. L. supervised the work. A. W. and X. T. drafted the manuscript. A. W. performed all data collection. E. F. and X. T. built the model and X. T. carried out the computational work.

## CONFLICTS OF INTEREST

The authors declare that there are no conflicts of interest.

## ORCID

Alexandra Westbrook  <http://orcid.org/0000-0002-8506-4737>

Xun Tang  <http://orcid.org/0000-0003-0317-9176>

Colin S. Maxwell  <http://orcid.org/0000-0002-8756-6255>

James Chappell  <http://orcid.org/0000-0001-7367-1524>

Mary J. Dunlop  <http://orcid.org/0000-0002-9261-8216>

Vincent Noireaux  <http://orcid.org/0000-0002-5213-273X>

Chase L. Beisel  <http://orcid.org/0000-0003-0650-9943>

Julius Lucks  <http://orcid.org/0000-0002-0619-6505>

Elisa Franco  <http://orcid.org/0000-0003-1103-2668>

## REFERENCES

- Agrawal, D. K., Tang, X., Westbrook, A., Marshall, R., Maxwell, C. S., & Lucks, J., et al. (2018). Mathematical modeling of RNA-based architectures for closed loop control of gene expression. *ACS Synthetic Biology*, 7(5), 1219–1228. <https://doi.org/10.1021/acssynbio.8b00040>
- Alon, U. (2013). *An introduction to systems biology*. Chapman & Hall/CRC.
- Barone, F., Dorr, F., Marasco, L. E., Mildiner, S., Patop, I. L., Sosa, S., ... Nadra, A. D. (2017). Design and evaluation of an incoherent feed-forward loop for an arsenic biosensor based on standard iGEM parts. *Synthetic Biology*, 2(1), 802. <https://doi.org/10.1093/synbio/ysx006>
- Basu, S., Mehreja, R., Thiberge, S., Chen, M. -T., & Weiss, R. (2004). Spatiotemporal control of gene expression with pulse-generating networks. *Proceedings of the National Academy of Sciences of the United States of America*, 101(17), 6355–6360. <https://doi.org/10.1073/pnas.0307571101>
- Beisel, C. L., & Storz, G. (2010). Base pairing small RNAs and their roles in global regulatory networks. *FEMS Microbiology Reviews*, 34(5), 866–882. <https://doi.org/10.1111/j.1574-6976.2010.00241.x>
- Bikard, D., Jiang, W., Samai, P., Hochschild, A., Zhang, F., & Marraffini, L. A. (2013). Programmable repression and activation of bacterial gene expression using an engineered CRISPR-Cas system. *Nucleic Acids Research*, 41(15), 7429–7437. <https://doi.org/10.1093/nar/gkt520>
- Boyle, E. A., Andreasson, J. O. L., Chircus, L. M., Sternberg, S. H., Wu, M. J., Guegler, C. K., ... Greenleaf, W. J. (2017). High-throughput biochemical profiling reveals sequence determinants of dCas9 off-target binding and unbinding. *Proceedings of the National Academy of Sciences of the United States of America*, 114(21), 5461–5466. <https://doi.org/10.1073/pnas.1700557114>
- Brown, K. S., & Sethna, J. P. (2003). Statistical mechanical approaches to models with many poorly known parameters. *Physical Review. E, Statistical, Nonlinear, and Soft Matter Physics*, 68(2 Pt 1), 021904. <https://doi.org/10.1103/PhysRevE.68.021904>
- Carrier, T. A., & Keasling, J. D. (1999). Library of synthetic 5' secondary structures to manipulate mRNA stability in *Escherichia coli*. *Biotechnology Progress*, 15(1), 58–64. <https://doi.org/10.1021/bp9801143>
- Chappell, J., Takahashi, M. K., & Lucks, J. B. (2015). Creating small transcription activating RNAs. *Nature Chemical Biology*, 11(3), 214–220. <https://doi.org/10.1038/nchembio.1737>
- Chappell, J., Takahashi, M. K., Meyer, S., Loughrey, D., Watters, K. E., & Lucks, J. (2013). The centrality of RNA for engineering gene expression. *Biotechnology Journal*, 8(12), 1379–1395. <https://doi.org/10.1002/biot.201300018>
- Chappell, J., Westbrook, A., Verosloff, M., & Lucks, J. B. (2017). Computational design of small transcription activating RNAs for versatile and dynamic gene regulation. *Nature Communications*, 8(1), 795. <https://doi.org/10.1038/s41467-017-01082-6>
- Cheng, Y.-Y., Hirning, A. J., Josić, K., & Bennett, M. R. (2017). The Timing of Transcriptional Regulation in Synthetic Gene Circuits. *ACS Synthetic Biology*, 6(11), 1996–2002. <https://doi.org/10.1021/acssynbio.7b00118>
- Del Vecchio, D., & Murray, R. M. (2017). *Biomolecular feedback systems* (1). Princeton, NJ: Princeton University Press. <https://doi.org/10.23943/princeton/9780691161532.001.0001>
- Deltcheva, E., Chylinski, K., Sharma, C. M., Gonzales, K., Chao, Y., Pirzada, Z. A., ... Charpentier, E. (2011). CRISPR RNA maturation by trans-encoded small RNA and host factor RNase III. *Nature*, 471(7340), 602–607. <https://doi.org/10.1038/nature09886>
- Duschak, V. G. (2015). Synthetic biology: Computational modeling bridging the gap between in vitro and in vivo reactions. *Current Synthetic and Systems Biology*, 3(3) <https://doi.org/10.4172/2332-0737.1000127>
- Entus, R., Aufderheide, B., & Sauro, H. M. (2007). Design and implementation of three incoherent feed-forward motif based biological concentration sensors. *Systems and Synthetic Biology*, 1(3), 119–128. <https://doi.org/10.1007/s11693-007-9008-6>
- Gander, M. W., Vrana, J. D., Voje, W. E., Carothers, J. M., & Klavins, E. (2017). Digital logic circuits in yeast with CRISPR-dCas9 NOR gates. *Nature Communications*, 8, 15459. <https://doi.org/10.1038/ncomms15459>
- Garamella, J., Marshall, R., Rustad, M., & Noireaux, V. (2016). The all *E. coli* TX-TL Toolbox 2.0: A platform for cell-free synthetic biology. *ACS Synthetic Biology*, 5(4), 344–355. <https://doi.org/10.1021/acssynbio.5b00296>
- Goentoro, L., Shoval, O., Kirschner, M. W., & Alon, U. (2009). The incoherent feedforward loop can provide fold-change detection in gene regulation. *Molecular Cell*, 36(5), 894–899. <https://doi.org/10.1016/j.molcel.2009.11.018>
- Green, A. A., Silver, P. A., Collins, J. J., & Yin, P. (2014). Toehold switches: De-novo-designed regulators of gene expression. *Cell*, 159(4), 925–939. <https://doi.org/10.1016/j.cell.2014.10.002>
- Gupta, A., Reizman, I. M. B., Reisch, C. R., & Prather, K. L. J. (2017). Dynamic regulation of metabolic flux in engineered bacteria using a pathway-independent quorum-sensing circuit. *Nature Biotechnology*, 35(3), 273–279. <https://doi.org/10.1038/nbt.3796>
- Hu, C. Y., Takahashi, M. K., Zhang, Y., & Lucks, J. B. (2018). Engineering a functional small RNA negative autoregulation network with model-guided design. *ACS Synthetic Biology*, 7, 7b00440–1518b00440. <https://doi.org/10.1021/acssynbio.7b00440>

- Hu, C. Y., Varner, J. D., & Lucks, J. B. (2015). Generating effective models and parameters for RNA genetic circuits. *ACS Synthetic Biology*, 4(8), 914–926. <https://doi.org/10.1021/acssynbio.5b00077>
- Jinek, M., Chylinski, K., Fonfara, I., Hauer, M., Doudna, J. A., & Charpentier, E. (2012). A programmable dual-RNA-guided DNA endonuclease in adaptive bacterial immunity. *Science*, 337(6096), 816–821. <https://doi.org/10.1126/science.1225829>
- Kaplan, S., Bren, A., Dekel, E., & Alon, U. (2008). The incoherent feed-forward loop can generate non-monotonic input functions for genes. *Molecular Systems Biology*, 4(1), 203. <https://doi.org/10.1038/msb.2008.43>
- Liao, C., Blanchard, A. E., & Lu, T. (2017). An integrative circuit-host modelling framework for predicting synthetic gene network behaviours. *Nature Microbiology*, 2(12), 1658–1666. <https://doi.org/10.1038/s41564-017-0022-5>
- Lucks, J. B., Qi, L., Mutalik, V. K., Wang, D., & Arkin, A. P. (2011). Versatile RNA-sensing transcriptional regulators for engineering genetic networks. *Proceedings of the National Academy of Sciences of the United States of America*, 108(21), 8617–8622. <https://doi.org/10.1073/pnas.1015741108>
- Lucks, J. B., Qi, L., Whitaker, W. R., & Arkin, A. P. (2008). Toward scalable parts families for predictable design of biological circuits. *Current Opinion in Microbiology*, 11(6), 567–573. <https://doi.org/10.1016/j.mib.2008.10.002>
- Mangan, S., & Alon, U. (2003). Structure and function of the feed-forward loop network motif. *Proceedings of the National Academy of Sciences of the United States of America*, 100(21), 11980–11985. <https://doi.org/10.1073/pnas.2133841100>
- Mangan, S., Itzkovitz, S., Zaslaver, A., & Alon, U. (2006). The incoherent feed-forward loop accelerates the response-time of the gal system of *Escherichia coli*. *Journal of Molecular Biology*, 356(5), 1073–1081. <https://doi.org/10.1016/j.jmb.2005.12.003>
- Marshall, R., Maxwell, C. S., Collins, S. P., Jacobsen, T., Luo, M. L., Begemann, M. B., ... Noireaux, V. (2018). Rapid and scalable characterization of CRISPR technologies using an *E. coli* cell-free transcription-translation system. *Molecular Cell*, 69(1), 146–157. <https://doi.org/10.1016/j.molcel.2017.12.007>
- Mekler, V., Minakhin, L., Semenova, E., Kuznedelov, K., & Severinov, K. (2016). Kinetics of the CRISPR-Cas9 effector complex assembly and the role of 3'-terminal segment of guide RNA. *Nucleic Acids Research*, 44(6), 2837–2845. <https://doi.org/10.1093/nar/gkw138>
- Milo, R. (2002). Network motifs: Simple building blocks of complex networks. *Science*, 298(5594), 824–827. <https://doi.org/10.1126/science.298.5594.824>
- Mishra, D., Rivera, P. M., Lin, A., Del Vecchio, D., & Weiss, R. (2014). A load driver device for engineering modularity in biological networks. *Nature Biotechnology*, 32(12), 1268–1275. <https://doi.org/10.1038/nbt.3044>
- Nielsen, A. A. K., Der, B. S., Shin, J., Vaidyanathan, P., Paralanov, V., Strychalski, E. A., ... Voigt, C. A. (2016). Genetic circuit design automation. *Science*, 352(6281), aac7341. <https://doi.org/10.1126/science.aac7341>
- O'Brien, E. L., Van itallie, E., & Bennett, M. R. (2012). Modeling synthetic gene oscillators. *Mathematical Biosciences*, 236(1), 1–15. <https://doi.org/10.1016/j.mbs.2012.01.001>
- Osella, M., Bosia, C., Corá, D., & Caselle, M. (2011). The role of incoherent microRNA-mediated feedforward loops in noise buffering. *PLOS Computational Biology*, 7(3), e1001101. <https://doi.org/10.1371/journal.pcbi.1001101>
- Qi, L. S., Larson, M. H., Gilbert, L. A., Doudna, J. A., Weissman, J. S., Arkin, A. P., & Lim, W. A. (2013). Repurposing CRISPR as an RNA-guided platform for sequence-specific control of gene expression. *Cell*, 152(5), 1173–1183. <https://doi.org/10.1016/j.cell.2013.02.022>
- Qian, Y., Huang, H. -H., Jiménez, J. I., & Del Vecchio, D. (2017). Resource competition shapes the response of genetic circuits. *ACS Synthetic Biology*, 6(7), 1263–1272. <https://doi.org/10.1021/acssynbio.6b00361>
- Shen-Orr, S. S., Milo, R., Mangan, S., & Alon, U. (2002). Network motifs in the transcriptional regulation network of *Escherichia coli*. *Nature Genetics*, 31(1), 64–68. <https://doi.org/10.1038/ng881>
- Subsoontorn, P., Kim, J., & Winfree, E. (2012). Ensemble Bayesian analysis of bistability in a synthetic transcriptional switch. *ACS Synthetic Biology*, 1(8), 299–316. <https://doi.org/10.1021/sb300018h>
- Sun, Z. Z., Hayes, C. A., Shin, J., Caschera, F., Murray, R. M., & Noireaux, V. (2013). Protocols for implementing an *Escherichia coli*-based TX-TL cell-free expression system for synthetic biology. *Journal of Visualized Experiments: JoVE*, 79, e50762. <https://doi.org/10.3791/50762>
- Takahashi, M. K., Chappell, J., Hayes, C. A., Sun, Z. Z., Kim, J., Singhal, V., ... Lucks, J. B. (2015). Rapidly characterizing the fast dynamics of RNA genetic circuitry with cell-free transcription-translation (TX-TL) systems. *ACS Synthetic Biology*, 4(5), 503–515. <https://doi.org/10.1021/sb400206c>
- Takahashi, M. K., Hayes, C. A., Chappell, J., Sun, Z. Z., Murray, R. M., Noireaux, V., & Lucks, J. B. (2015). Characterizing and prototyping genetic networks with cell-free transcription-translation reactions. *Methods*, 86, 60–72. <https://doi.org/10.1016/j.ymeth.2015.05.020>
- Takahashi, M. K., Watters, K. E., Gasper, P. M., Abbott, T. R., Carlson, P. D., Chen, A. A., & Lucks, J. B. (2016). Using in-cell SHAPE-Seq and simulations to probe structure-function design principles of RNA transcriptional regulators. *RNA*, 22(6), 920–933. <https://doi.org/10.1261/rna.054916.115>
- Wright, A. V., Sternberg, S. H., Taylor, D. W., Staahl, B. T., Bardales, J. A., Kornfeld, J. E., & Doudna, J. A. (2015). Rational design of a split-Cas9 enzyme complex. *Proceedings of the National Academy of Sciences of the United States of America*, 112(10), 2984–2989. <https://doi.org/10.1073/pnas.1501698112>

## SUPPORTING INFORMATION

Additional supporting information may be found online in the Supporting Information section at the end of the article.

**How to cite this article:** Westbrook A, Tang X, Marshall R, et al. Distinct timescales of RNA regulators enable the construction of a genetic pulse generator. *Biotechnology and Bioengineering*. 2019;1–13. <https://doi.org/10.1002/bit.26918>

## Supporting Information for

# Distinct timescales of RNA regulators enable the construction of a genetic pulse generator

Alexandra Westbrook<sup>1,§</sup>, Xun Tang<sup>2,§</sup>, Ryan Marshall<sup>3</sup>, Colin S. Maxwell<sup>4</sup>, James Chappell<sup>5</sup>, Deepak K. Agrawal<sup>6</sup>, Mary J. Dunlop<sup>6</sup>, Vincent Noireaux<sup>3</sup>, Chase L. Beisel<sup>4,7,8</sup>, Julius Lucks<sup>9,\*</sup>, and Elisa Franco<sup>2,\*</sup>

<sup>1</sup>Robert F. Smith School of Chemical and Biomolecular Engineering, Cornell University, Ithaca, NY 14853, United States

<sup>2</sup>Department of Mechanical Engineering, University of California at Riverside, Riverside, CA 92521, United States

<sup>3</sup>School of Physics and Astronomy, University of Minnesota, Minneapolis, MN 55455, United States

<sup>4</sup>Department of Chemical and Biomolecular Engineering, North Carolina State University, Raleigh, NC 27695, United States

<sup>5</sup>Department of Biosciences, Rice University, Houston, TX 77005, United States

<sup>6</sup>Biomedical Engineering Department, Boston University, Boston, MA 02215, United States

<sup>7</sup>Helmholtz Institute for RNA-based Infection Research (HIRI), Josef-Schneider-Str. 2 / D15, D-97080 Würzburg, Germany

<sup>8</sup>Faculty of Medicine, University of Würzburg, Würzburg, Germany

<sup>9</sup>Department of Chemical and Biological Engineering, Northwestern University, Evanston, IL 60208, United States

	Description
Table S1	Parameter values used in Figure 3 and 5
Table S2	Important DNA sequences
Table S3	Plasmids used in this study
Figure S1	Complete CRISPRi pre-incubation data
Figure S2	Complete STAR parameterization data
Figure S3	Complete CRISPRi parameterization data
Figure S4	Parameter correlation comparison of the 1000 fitted STAR parameters
Figure S5	Parameter correlation comparison of the 1000 fitted CRISPRi parameters
Figure S6	Parameter sensitivity analysis of CRISPR, STAR, and Pulse generator.
Figure S7	Predictions of all combinations of STAR and CRISPRi parameter sets
Figure S8	Prediction parameters compared to fitting parameters
Figure S9	Best fitting from each of the 10 Bayesian inference for STAR
Note S1	Slope computation and fitting for Fig.2
Note S2	Bayesian inference Monte Carlo approach for parameterization.

**Table S1:** Parameter values used in Figure 3 and 5. The best fitting EGFP reporter parameters from both STAR and CRISPRi pre-incubation experiments are listed in order of STAR/CRISPRi.

Parameters	Varying Interval	Best Fitting Values	Best Prediction Values	Literature Reference
$\alpha_s$	$10^2 - 10^3 \text{ s}^{-1}$	2.038 $\text{s}^{-1}$	2.038 $\text{s}^{-1}$	2 $\text{s}^{-1}$ (Hu et al., 2015)
$\delta_s$	$10^{-4} - 10^{-1} \text{ s}^{-1}$	0.0915 $\text{s}^{-1}$	0.0915 $\text{s}^{-1}$	0.00002 $\text{s}^{-1}$ ~0.1 $\text{t}^{-1}$ (Schmid et al., 2018)
$\beta_s$	$10^3 - 10^6 \text{ nM}^{-1}\text{s}^{-1}$	310969 $\text{nM}^{-1}\text{s}^{-1}$	310969 $\text{nM}^{-1}\text{s}^{-1}$	N/A
$\alpha_{cr/tr}$	$10^2 - 10^3 \text{ s}^{-1}$	0.739 $\text{s}^{-1}$	0.03 $\text{s}^{-1}$	2 $\text{s}^{-1}$ (Hu et al., 2015)
$\delta_{cr}$	$10^{-4} - 10^{-1} \text{ s}^{-1}$	0.0615 $\text{s}^{-1}$	0.0614 $\text{s}^{-1}$	0.00002 $\text{s}^{-1}$ ~0.1 $\text{t}^{-1}$ (Schmid et al., 2018)
$\delta_{tr}$	$10^{-4} - 10^{-1} \text{ s}^{-1}$	0.030 $\text{s}^{-1}$	0.073 $\text{s}^{-1}$	0.00002 $\text{s}^{-1}$ ~0.1 $\text{t}^{-1}$ (Schmid et al., 2018)
$\delta_g$	$10^{-4} - 10^{-1} \text{ s}^{-1}$	0.085 $\text{s}^{-1}$	0.0176 $\text{s}^{-1}$	0.00002 $\text{s}^{-1}$ ~0.1 $\text{t}^{-1}$ (Schmid et al., 2018)
$\gamma_1$	$10^3 - 10^6 \text{ nM}^{-1}\text{s}^{-1}$	$7.38 \times 10^6 \text{ nM}^{-1}\text{s}^{-1}$	$8.69 \times 10^6 \text{ nM}^{-1}\text{s}^{-1}$	N/A
$\gamma_2$	$10^3 - 10^6 \text{ nM}^{-1}\text{s}^{-1}$	$6.56 \times 10^6 \text{ nM}^{-1}\text{s}^{-1}$	$3.68 \times 10^6 \text{ nM}^{-1}\text{s}^{-1}$	N/A
$\omega$	$10^3 - 10^6 \text{ nM}^{-1}\text{s}^{-1}$	$3.1 \times 10^6 \text{ nM}^{-1}\text{s}^{-1}$	$7.17 \times 10^6 \text{ nM}^{-1}\text{s}^{-1}$	N/A
$\alpha_m$	$10^1 - 100 \text{ s}^{-1}$	0.1/50.65 $\text{s}^{-1}$	0.1 $\text{s}^{-1}$	2 $\text{s}^{-1}$ (Hu et al., 2015)
$\delta_m$	$10^{-4} - 10^{-1} \text{ s}^{-1}$	$4.01 \times 10^{-2}$ /0.094 $\text{s}^{-1}$	$4.01 \times 10^{-2} \text{ s}^{-1}$	0.00002 $\text{s}^{-1}$ ~0.1 $\text{t}^{-1}$ (Schmid et al., 2018)
$K_i$	$10^{-4} - 10^{-2} \text{ s}^{-1}$	0.0012/9.019 $\times 10^{-4} \text{ s}^{-1}$	0.0012 $\text{s}^{-1}$	~0.0023 $\text{s}^{-1}$ (Hu et al., 2015)
$K_e$	$10^{-4} - 10^{-2} \text{ s}^{-1}$	0.009/4.168 $\times 10^{-4} \text{ s}^{-1}$	0.009 $\text{s}^{-1}$	~0.0013 $\text{s}^{-1}$ (Hu et al., 2015)
$\alpha_{gm}$	$10^1 - 10^4 \text{ s}^{-1}$	0.092/0.015 $\text{s}^{-1}$	0.092 $\text{s}^{-1}$	~0.05 $\text{s}^{-1}$ (Hu et al., 2015)

**Table S2:** Important DNA sequences

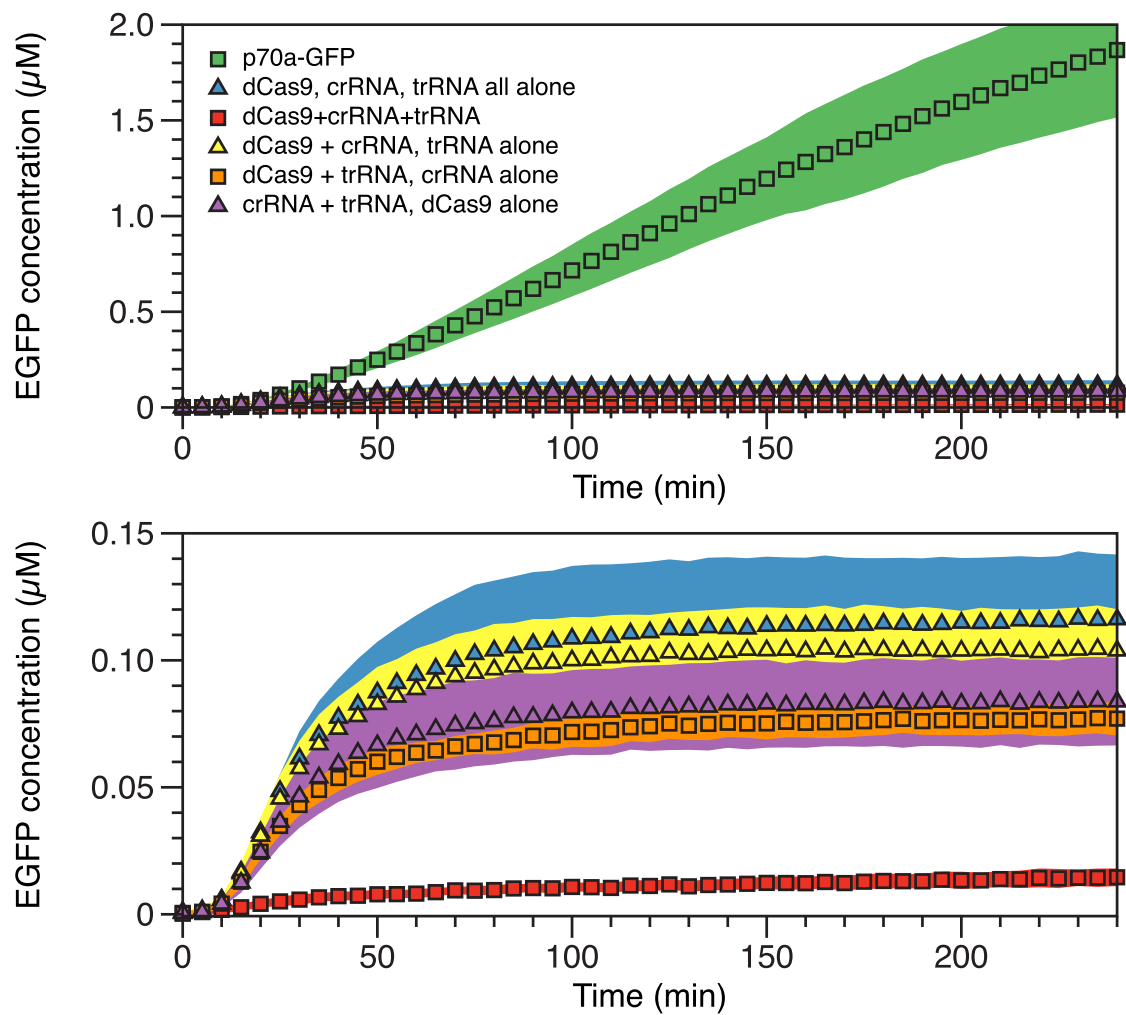
Name	Sequence
J23119	TTGACAGCTAGCTCAGTCCTAGGTATAATACTAGT
p70a	TGAGCTAACACCGTGCGTGTGACAATTTTACCTCTGGCGGTGATAATGGTTGC A
STAR 5	TGAACTGTATACATTCCCCGCAGGATAGGAATTGAAGATGAAACGATGAGACT TGGGACGAGGATCT
STAR 5	TCGICCCAAGTCTCATCGTTTCATCTTCAATTCCTATCCTGCGGGGAATGTATAC
Target	AGTTCATGTATATATTCCCCGCTTTTTTTTGGATCT
crRNA	GGTAAAATTGTCAACACGCAGTTTTAGAGCTATGCTGTTTTGAATGGTCCCAA AC
Scrambled crRNA	AAGCAGATTACGTTCAAGCAGTTTTAGAGCTATGCTGTTTTGAATGGTCCCAA AC
tracrRNA	ATCTTGTTGGAACCAATTCAAAACAGCATAGCAAGTTAAAATAAGGCTAGTCCG TTATCAACTTGAAAAAGTGGCACCGAGTCGGTGCTTTTTTTG
eGFP (Ribosome binding site (RBS) - GFP)	AGAAGGAGATATACCATGGAGCTTTTCACTGGCGTTGTTCCCATCCTGGTTCGAG CTGGACGGCGACGTAAACGGCCACAAGTTCAGCGTGTCCGGCGAGGGCGAGG GCGATGCCACCTACGGCAAGCTGACCCTGAAGTTCATCTGCACCACCGGCAAG CTGCCCGTGCCCTGGCCACCCTCGTGACCACCCTGACCTACGGCGTGCAGTGC TTCAGCCGCTACCCCGACCACATGAAGCAGCACGACTTCTTCAAGTCCGCCATG CCCGAAGGCTACGTCCAGGAGCGCACCATCTTCTTCAAGGACGACGGCAACTA CAAGACCCGCGCCGAGGTGAAGTTCGAGGGCGACACCCTGGTGAACCGCATCG AGCTGAAGGGCATCGACTTCAAGGAGGACGGCAACATCCTGGGGCACAAGCTG GAGTACAACACTACAACAGCCACAACGTCTATATCATGGCCGACAAGCAGAAGAA CGGCATCAAGGTGAACTTCAAGATCCGCCACAACATCGAGGACGGCAGCGTGC AGCTCGCCGACCACTACCAGCAGAACACCCCATCGGCGACGGCCCCGTGCTG CTGCCCGACAACCACTACCTGAGCACCCAGTCCGCCCTGAGCAAAGACCCCAA CGAGAAGCGCGATCACATGGTCCTGCTGGAGTTCGTGACCGCCCGCCGGGATCT AACTCGAG



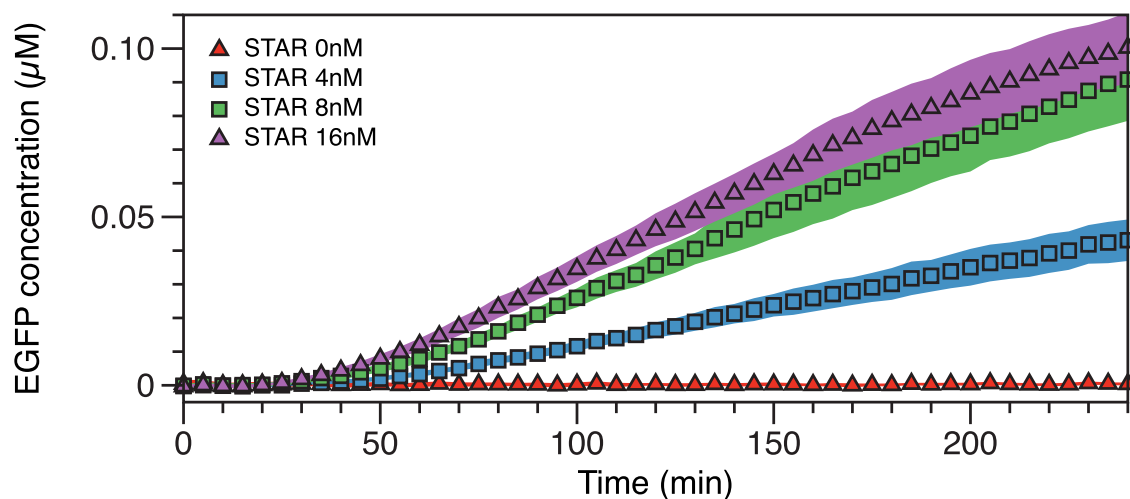
TrnB	GAAGCTTGGGCCCGAACAAAACTCATCTCAGAAGAGGATCTGAATAGCGCCG TCGACCATCATCATCATCATTGAGTTTAAACGGTCTCCAGCTTGGCTGTTTT GGCGGATGAGAGAAGATTTTCAGCCTGATACAGATTAATCAGAACGCAGAAG CGGTCTGATAAAACAGAATTTGCCTGGCGGCAGTAGCGCGGTGGTCCCACCTG ACCCCATGCCGAACCTCAGAAGTGAAACGCCGTAGCGCCGATGGTAGTGTGGGG TCTCCCATGCGAGAGTAGGGAACCTGCCAGGCATCAAATAAAACGAAAGGCTC AGTCGAAAGACTGGGCCTTTCGTTTTATCTGTTGTTTGTGCGGTGAACT
T500	CAAAGCCCGCCGAAAGGGCGGGCTTTT

**Table S3:** Plasmids used in this study. Sequences in the plasmid architecture can be found in Table S2.

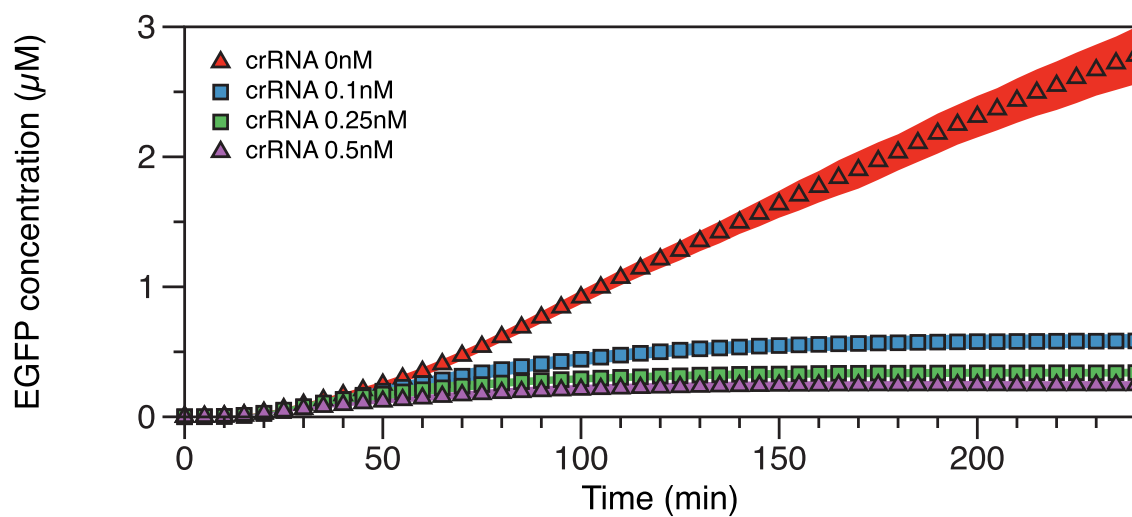
Plasmid #	Plasmid architecture	Name	Figure	Reference
JBL002	J23119 – TrnB – ColE1 origin – AmpR	No STAR control	2-6, S2-5, S7, S10	A
70a-GFP	p70a – GFP – ColE1 origin - AmpR	P70a-GFP	2	Garamella et al. 2016
AMW019	p70a – STAR 5 Target – GFP – ColE1 origin - AmpR	P70a-STAR Target-GFP	2, 4, 5, S4, S5, S7	This paper
JBL4971	J23119 – STAR 5 – t500 – ColE1 origin - AmpR	STAR 5	2, 4, S5, S10	Chappell et al. 2017
CSM257	J23119 – crRNA – t500 – CamR – ColE1	crRNA	4	This paper
CSM258	J23119 – scrambled crRNA – t500 – CamR – ColE1	crRNA control	4, 5, S7	This paper
CSM275	J23119 – tracrRNA – t500 – CamR – ColE1	tracrRNA	4	This paper



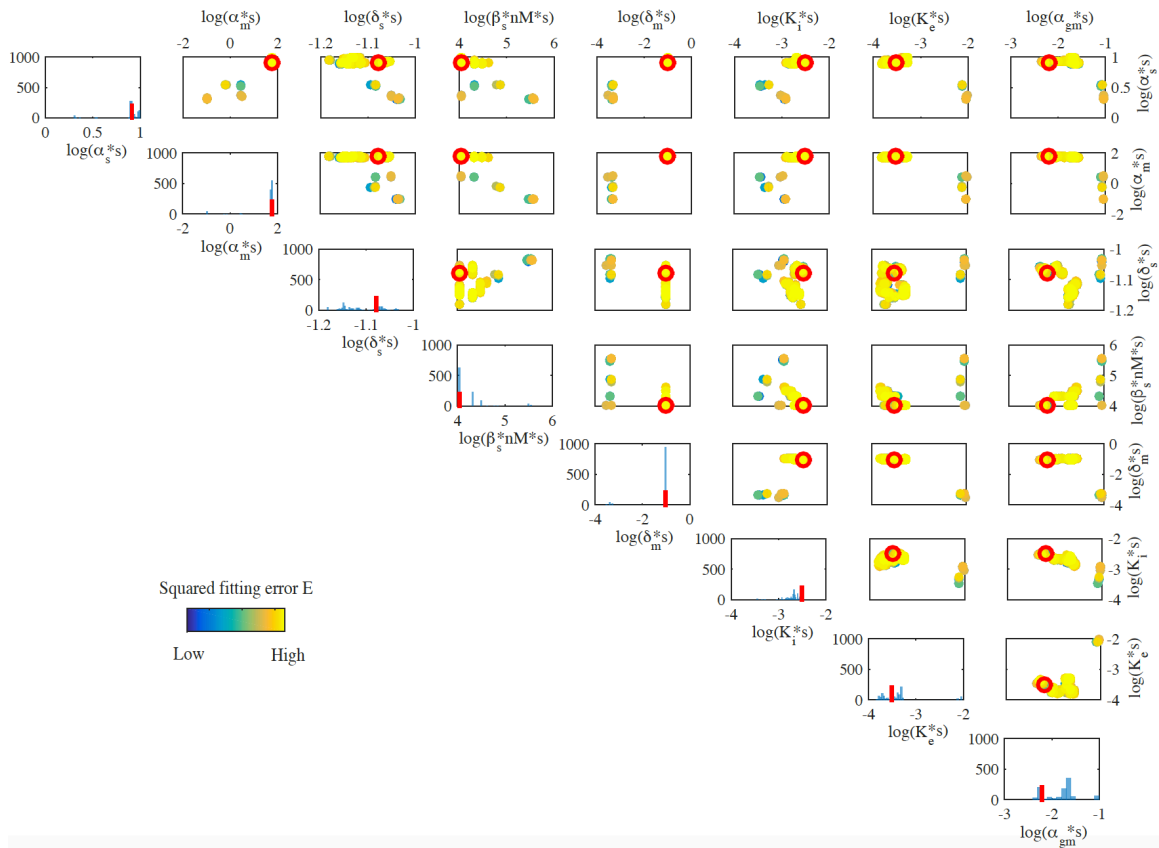
**Supplementary Figure S1:** Complete data for the CRISPRi pre-incubation experiment. Functional time course characterization of the CRISPRi response when parts are incubated together or alone in various combinations for 2 hours before measurements. When no crRNA or trRNA is present, GFP expression is ON (green). When all the parts are incubated together, GFP is quickly repressed (red). GFP repression is delayed when all parts are incubated separately (blue). Incubating trRNA alone, but dCas9 and crRNA together shows similar delays in repression (yellow). When crRNA (orange) or dCas9 (purple) is incubated alone (but dCas9 and trRNA together or crRNA and trRNA together, respectively) the delay is less dramatic. The colored region indicates the standard deviation of nine replicates. The same data is shown in both plots except the p70a-GFP has been removed from the bottom plot so that the other conditions could be seen clearly.



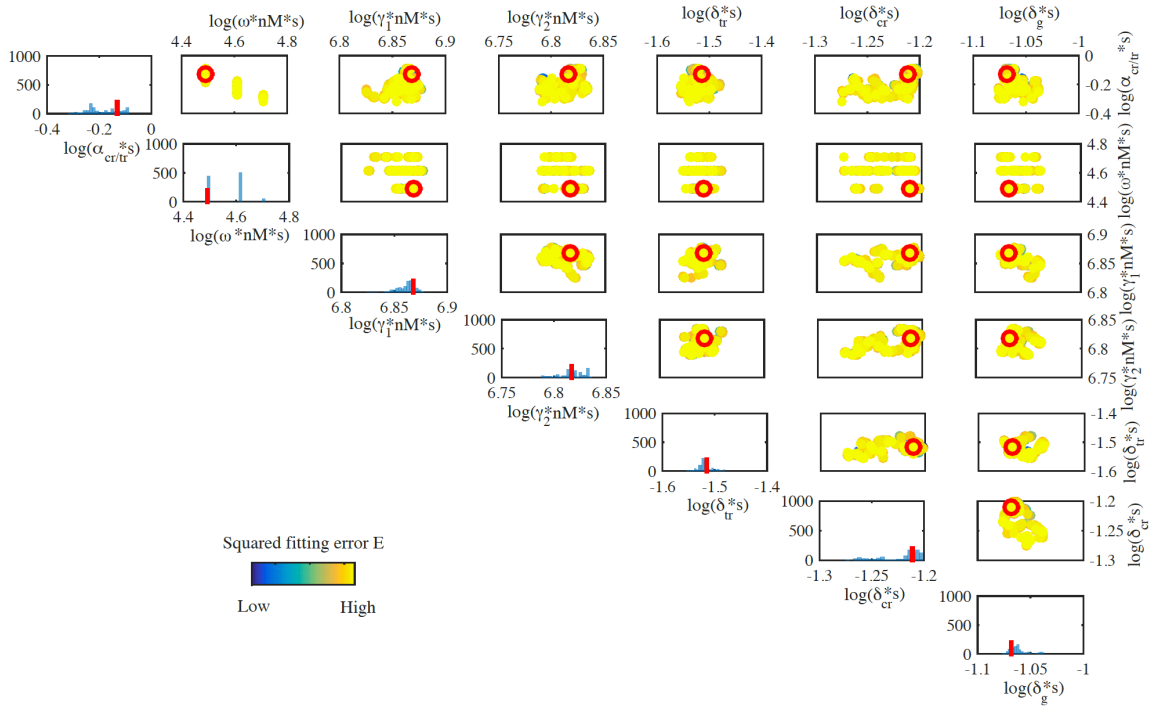
**Supplementary Figure S2:** Complete data for the STAR parameterization experiment. Functional time course characterization of GFP expression when different concentrations of STAR plasmid is added to the TXTL reaction with 0.5nM of the p70a-STAR Target-GFP plasmid at the start of the measurement. The colored region indicates the standard deviation of nine replicates.



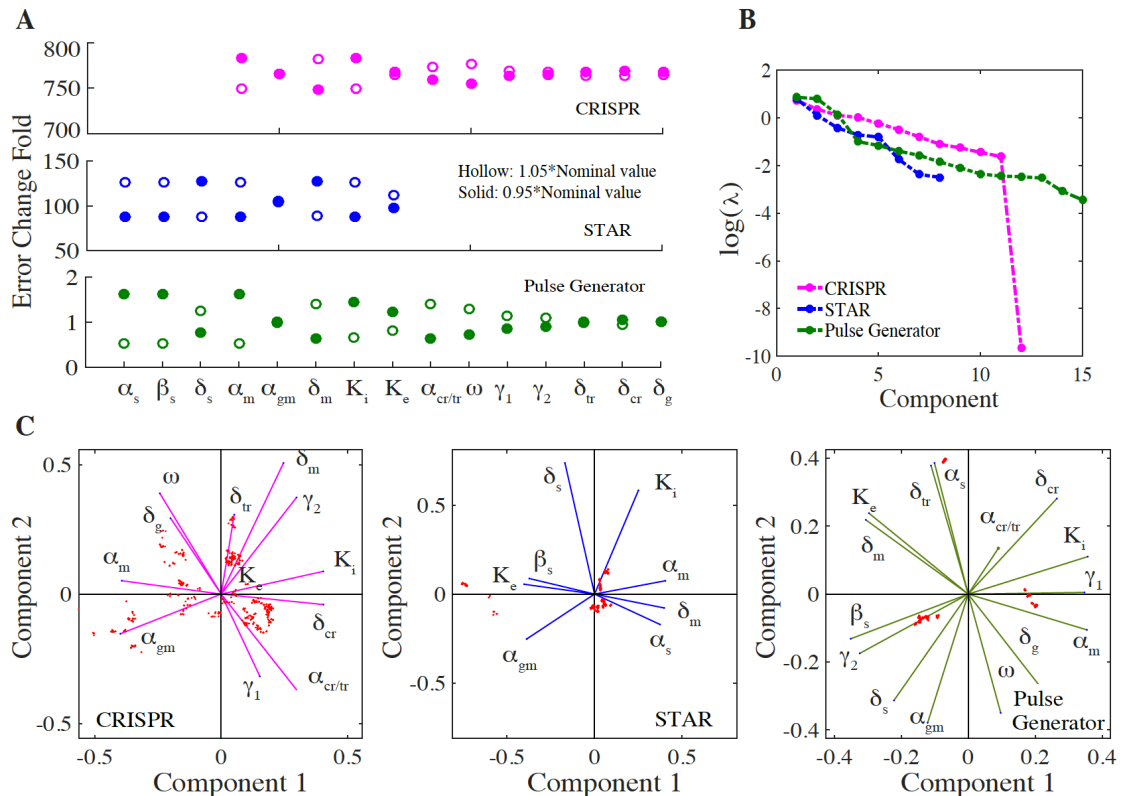
**Supplementary Figure S3:** Complete data for the CRISPRi parameterization experiment. Functional time course characterization of GFP expression when different concentrations of crRNA and trRNA plasmids are added to the dCas9 TXTL reaction with 0.5nM of the p70a-GFP plasmid at the start of the measurement. The colored region indicates the standard deviation of nine replicates.



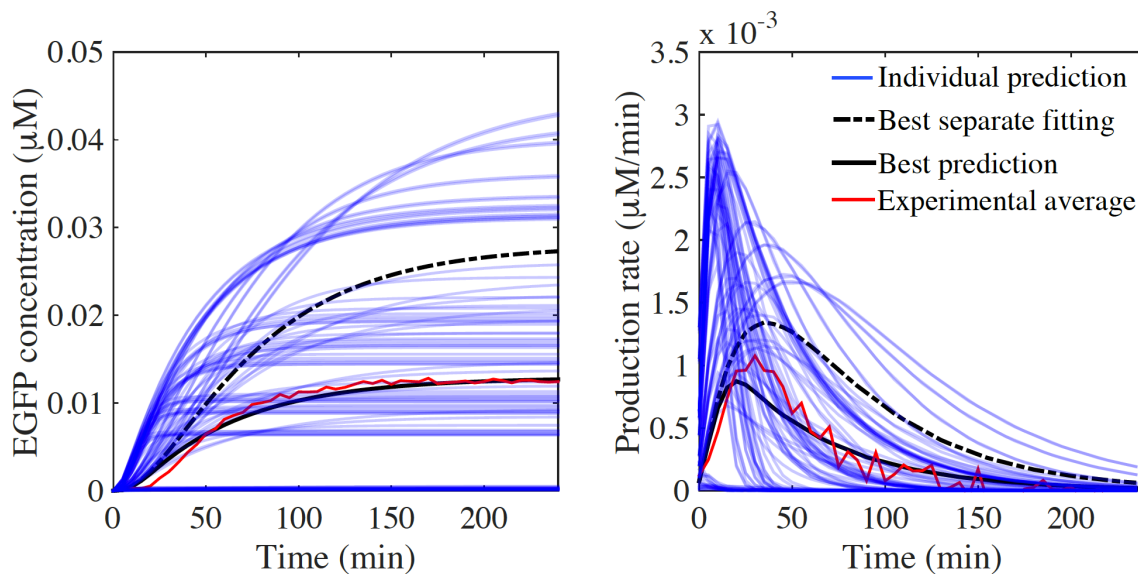
**Supplementary Figure S4:** Distribution and parameter correlation comparison of the 1000 fitted STAR parameters that gave the lowest fitting error to the STAR experiments. While no strong correlations were observed among the parameters, some parameters have a wider distribution such as  $\beta_s$  and  $K_i$ , some others have narrower distributions such as  $\alpha_m$ .



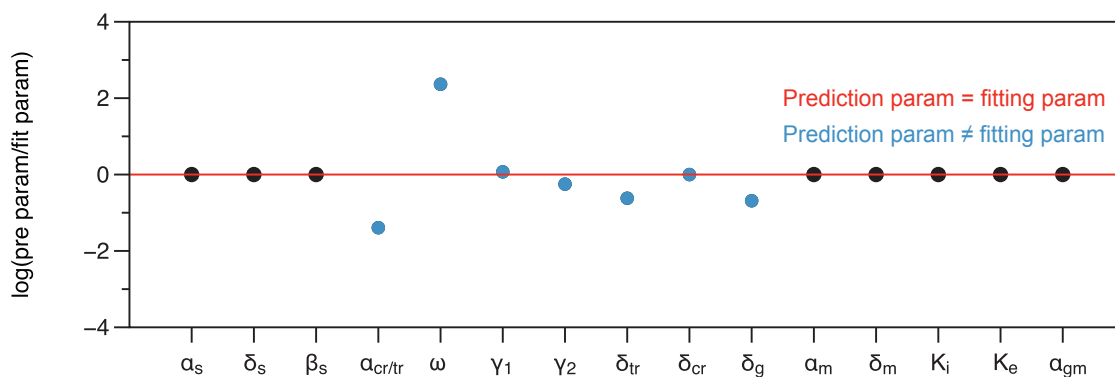
**Supplementary Figure S5:** Distribution and parameter correlation of the 1000 fitted CRISPRi parameters that gave the lowest fitting error to the CRISPRi experiments. While minimal to no correlations were observed among the parameters, some parameters have a wider distribution such as  $\gamma_1$ , some others have narrower distributions such as  $\omega$ .



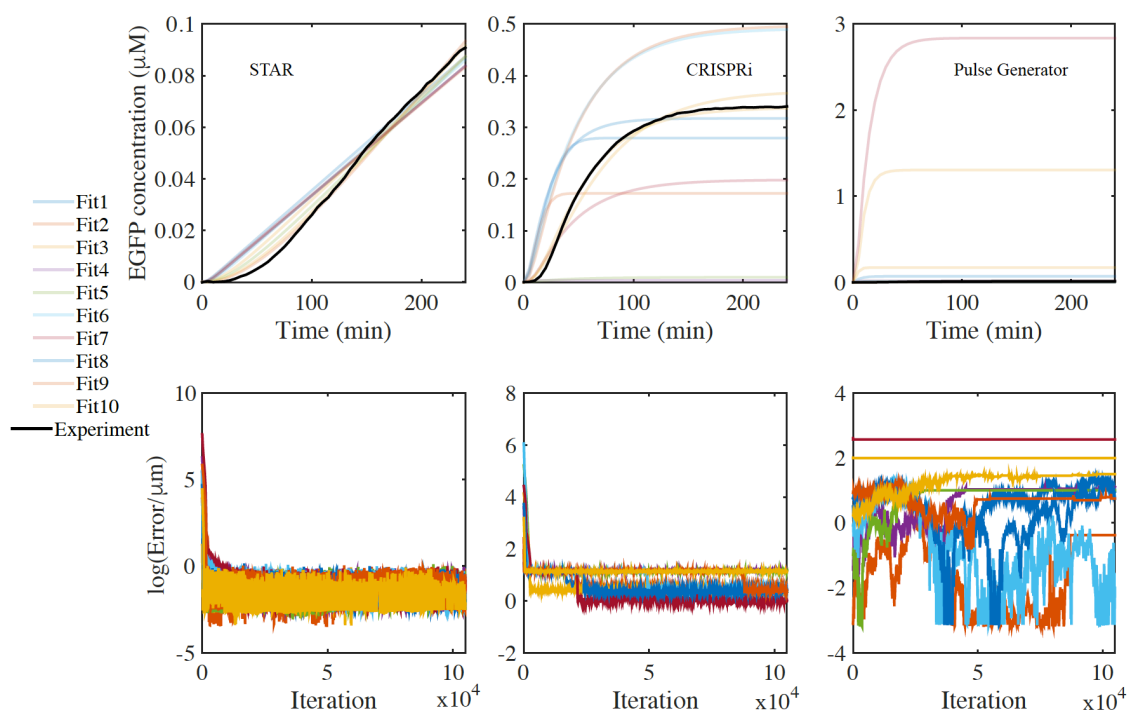
**Supplementary Figure S6:** Parameter sensitivity analysis of CRISPR, STAR, and Pulse generator. (A) Model fitting error subjects to +5% (hollow circles) and -5% (solid circles) of nominal parameter values (i.e. values gave the best fitting). Error is defined as in Eqn. 2 and is normalized over the fitting error with nominal parameters. While all three models show sensitivity over some parameters (e.g. EGFP production and maturation parameters), the CRISPR model shows the highest sensitivity to parameter values overall, while the combined pulse generator shows the lowest fitting error in all. This is because the pulse nominal fitting error is the highest, indicating non-convergence in the original fitting, and the CRISPR has a moderate nominal fitting error, since the original fitting is still converging. (B) Eigenvalue of principal component analysis of the 1000 sets of parameters that gave the lowest fitting error for CRISPR, STAR, and Pulse generator. All the eigenvalue plots indicate low correlation among each parameter, which is consistent with observations in Supplementary Figure S4 and 5. (C) Parameter projections in the first two components indicate the contribution of each parameter to the first principal components.



**Supplementary Figure S7:** Predictions of all the 100 combinations of STAR and CRISPRi separately fitted parameter sets demonstrate pulse in the combined model. Solid blue plots are individual predictions, dashed black plot is the prediction with the best separately fitted parameters, the solid black plot is the best prediction out of this 100 combinations, and the solid red plot is the averaged experimental measurement.



**Supplementary Figure S8:** Comparison in terms of parameter values in the best fitted and prediction parameter sets, demonstrating that a faster CRISPRi repressor formation rate was needed in the pulse circuit model for better prediction accuracy.



**Supplementary Figure S9:** Best fitting from each of the 10 Bayesian inference for STAR (a), CRISPRi (b), and pulse generator model (c). Fitting error demonstrates convergence comparison in log scale for STAR (e), CRISPRi (f), and pulse generator (h). There are 8, 12, and 15 parameters fitted in the STAR, CRISPRi, and pulse generator model respectively. Due to the increased number of parameters, even with a larger number of iterations it was challenging to obtain convergence for the CRISPRi and pulse model fitting, with worse fitting performance with respect to STAR. This indicates that our fitting approach becomes more challenging and computationally expensive as the number of fitted parameters increases.

### Supplementary Note S1: Slope computation and fitting for Fig.2 in the main manuscript.

Data were first smoothed by employing a 2-point moving average filter with MATLAB. The slope of each kinetic data set was computed using the MATLAB function `diff`. The slope was then averaged over all the available samples. The averaged slope was fitted to the following functions, using MATLAB's `lsqcurvefit` routine:

a) STAR system:

$$s(t) = d_1(1 - e^{-\frac{t}{d_2}})$$

Fitted values for the parameters are:  $d_1 = 0.3 \cdot 10^{-3} \mu\text{m}/\text{min}$ ,  $d_2 = 25 \text{ min}$ .

b) CRISPR system:

$$c(t) = k_1(e^{-\frac{t}{k_2}}) + k_3(e^{-\frac{t}{k_4}})$$

Fitted values for the parameters are:  $k_1 = -0.0218 \mu\text{m}/\text{min}$ ,  $k_2 = 14.24 \text{ min}$ ,  $k_3 = 0.0224 \mu\text{m}/\text{min}$ ,  $k_4 = 18.27 \text{ min}$

We chose 70% and 30% of the steady state value to determine the timescale of activation and repression respectively. For an exponential process, 63% of the steady state is achieved in a time equal to the time constant of the system. We rounded this number to 70% for the STAR (activation) process. For the CRISPR (repression) system it is more challenging to choose a cutoff because both initial and final slopes are zero. we assumed that the peak of the slope curve corresponds to the maximum achievable, and for consistency with the choice of the STAR cutoff we looked at a 70% decrease from the peak.

### Supplementary Note S2: Bayesian inference Monte Carlo approach for parameterization.

The Bayesian inference Monte Carlo approach used in this study was adopted from Ref. Hu et al., 2015. Here we briefly summarize the proof of how the Metropolis Monte Carlo based approach can be used for Bayesian inference methods, please refer to the supplementary information of Ref. Subsoontorn et al., 2012 for the detailed discussion.

First, let  $(P(D|M(\hat{\theta})))$  be the probability that the proposed model with parameter vector  $\hat{\theta}$  will generate the observed data  $D = \{Y_n\}$  with initial conditions  $I_1, I_2, \dots, I_p$ . Then let the repeatability variance modeled as



Gaussian random measurement error  $\sigma$ , for each experimental measurement  $Y_n$ , then we have

$$P(Y_n | M(\hat{\theta})) = \frac{1}{\sqrt{2\pi}\sigma} \exp\left(-\frac{(y(t_n, \hat{\theta}) - Y_n)^2}{2\sigma^2}\right).$$

Further assuming each experiment as independent, and convert the product into sum, it can be shown that:

$$P(D | M(\hat{\theta})) = \prod_n \frac{1}{\sqrt{2\pi}\sigma} \exp\left(-\frac{(y(t_n, \hat{\theta}) - Y_n)^2}{2\sigma^2}\right) \propto \exp\left(-\frac{\sum_n (y(t_n, \hat{\theta}) - Y_n)^2}{2\sigma^2}\right) \propto \exp\left(-\frac{E}{2\sigma^2}\right)$$

where  $E$  is the cost function used in our optimization. The above equation is then a Boltzmann distribution with energy  $E$  and temperature  $T = 2\sigma^2$ .

Then one can estimate the conditional probability  $P(M(\hat{\theta}) | D)$  of the model with parameters  $\hat{\theta}$  given experiment measurement  $D$ , using Bayesian inference with a uniform a priori distribution for model parameters as:

$$P(M(\hat{\theta}) | D) = \frac{P(M(\hat{\theta})) \times P(D | M(\hat{\theta}))}{P(D)} \propto P(D | M(\hat{\theta})) \propto \exp\left(-\frac{E}{2\sigma^2}\right)$$

thus allowing us to use Metropolis criteria to generate parameter sets that is consistent with the Boltzmann distribution for the parameterization.

## REFERENCES

Schmid, M., Tudek, A., & Jensen, T. H. (2018). Simultaneous measurement of transcriptional and post-transcriptional parameters by 3' end RNA-seq. *Cell Reports*, 24, 2468–2478. <https://doi.org/10.1016/j.celrep.2018.07.104>